Adaptive-depth randomized measurement for fermionic observables

Kaiming Bian[1, 2, 3] and Bujiao Wu[1, 2, 3, *]

[1] *Shenzhen Institute for Quantum Science and Engineering, Southern University of Science and Technology, Shenzhen 518055, China*
[2] *International Quantum Academy, Shenzhen 518048, China*
[3] *Guangdong Provincial Key Laboratory of Quantum Science and Engineering, Southern University of Science and Technology, Shenzhen, 518055, China*

Accurate estimation of fermionic observables is essential for advancing quantum physics and chemistry. The fermionic classical shadow (FCS) method offers an efficient framework for estimating these observables without requiring a transformation into a Pauli basis for k-local Fermionic observables. However, the random matchgate circuits in FCS require linear-depth circuits with a brickwork structure, which presents significant challenges for near-term quantum devices with limited computational resources. To address this limitation, we introduce an adaptive-depth fermionic classical shadow (ADFCS) protocol designed to reduce the circuit depth while maintaining the sample complexity. Through theoretical analysis and numerical fitting, we establish that the required depth for approximating a fermionic observable H is upper bounded by $\mathcal{O}\left(\max\{d_{\text{int}}^2(H)/\log n, d_{\text{int}}(H)\}\right)$ when the locality k is a constant, where d_{int} is the interaction distance of H. We demonstrate the effectiveness of the ADFCS protocol through numerical experiments, which show similar accuracy to the traditional FCS method while requiring significantly fewer quantum resources. Additionally, we apply ADFCS to compute the expectation value of the Kitaev chain Hamiltonian, further validating its performance in practical scenarios. Our findings suggest that ADFCS enables more efficient quantum simulations when the locality k is constant, reducing circuit depth while preserving the sample complexity and offering a viable solution for near-term quantum devices.

I. INTRODUCTION

The simulation of strongly correlated fermionic systems is a fundamental application of quantum computing, playing a crucial role in advancing our understanding of quantum materials and chemical processes [1–6]. These systems, characterized by complex electron correlations and dynamics, demand precise computational techniques to capture their behavior. A key computational challenge is the calculation of expectation values, such as energy levels in fermionic Hamiltonians, which serve as essential descriptors of system properties. Quantum algorithms such as variational quantum eigensolver (VQE)[7, 8] and quantum Monte Carlo methods[9, 10] provide powerful tools for this task. However, they typically require a significant number of measurements to achieve accurate results.

The classical shadow (CS) algorithm [11] was introduced to give a classical estimator for a quantum state ρ. The CS algorithm is particularly suitable for estimating the linear properties of ρ, such as expectation values $\{\text{Tr}(\rho Q_i)\}_{i=1}^m$. The number of measurements required is $\mathcal{O}\left(\max_i \|Q_i\|_{\text{shadow}}^2 \log m/\varepsilon^2\right)$, where ε is the desired estimation error and $\|\cdot\|_{\text{shadow}}$ denotes the shadow norm, which depends on the unitary ensemble. However, for certain local fermionic observables, such as $\gamma_1\gamma_{2n}$, the shadow norm scales exponentially, rendering the CS algorithm inefficient. To address this limitation, fermionic classical shadow (FCS) algorithms [12–17] were developed. These algorithms primarily differ from the CS algorithm by using a Gaussian unitary ensemble rather than the Clifford group for randomness. Both Gaussian unitary and Clifford elements require polynomial-size quantum circuits, which become challenging for near-term quantum devices due to issues like gate noise and limited coherence time [18–23]. In response to this, several approaches have been proposed to design shallow-depth CS protocols [24–27]. However, for the FCS side, Zhao et al. [13] have proved that there does not exist subgroup $G \subseteq \text{Cl}_n \cap \mathbb{M}_n$ which has a better fermionic shadow norm, where Cl_n is the n-qubit Clifford group and $\mathbb{M}_n$ is the matchgate group. King et al. [28] also demonstrated that single-copy measurements require $\Omega\left(n^{k/2}/\varepsilon^2\right)$ copies of ρ in any classical shadow based protocol to achieve an ε-error estimation for k-local Majorana strings. An intriguing open question remains:

Is there an efficient shallow-depth FCS algorithm for specific sets of fermionic observables?

In this work, we identify the minimum circuit depth required by the FCS protocol for k-local Majorana strings with constant k. Beginning with 2-local Majorana strings, we derive an expression that characterizes the dependence of sample complexity on circuit depth. Building on these findings, we investigate the depth required to minimize sample complexity for general k-local Majorana strings.

Specifically, we propose an adaptive-depth fermionic classical shadow (ADFCS) algorithm for optimizing the depth of the brickwork random matchgate circuit, as shown in Fig. 1(a-b). Similar to the FCS algorithm, ADFCS applies a random matchgate circuit $U_{Q_{d^*}}$, where

* bujiaowu@gmail.com

$U_{Q_{d^*}}$ is sampled from the d^*-depth random matchgate set in a brickwork structure, and utilizes classical shadows to estimate the expectation value of an observable H. By Ref. [29], constructing a Haar-random matchgate circuit with a brickwork architecture requires $\mathcal{O}(n)$ depth.

In contrast, ADFCS adaptively selects the depth d^* based on the interaction distance of the observable and constructs the random matchgate circuit $U_{Q_{d^*}}$ accordingly. The depth d^* is bounded by $\mathcal{O}\left(\max\{d_{\text{int}}^2(H)/\log n, d_{\text{int}}(H)\}\right)$ where d_{int} is the interaction distance of the fermionic observable H. We introduce an auxiliary variable $\alpha_{S,d}$ which is inversely proportional to the sample complexity. Then, we give an expression for estimating the order of $\alpha_{S,d}$. This expression is obtained by modeling the variance as a random walk in response to variations in d, and selecting an appropriated d^* such that the summation of the random walk probability on certain sites is large enough. The probability summation is proportional to $\alpha_{S,d}$. For constant k, we provide a lower bound for the probability summation with numerical support, which provides a lower bound for $\alpha_{S,d}$, thereby yielding an upper bound on the sample complexity. Specifically, when $k = 2$, we obtain a tight estimate for $\alpha_{S,d}$. The interaction distance for many physical observables (such as the Kiteav chain Hamiltonian [30, 31] and transversal Ising Hamiltonian [30, 32]) is small since a particle can not interact with a remote particle. It suggests that the optimal depth d^* for these observables is relatively small, making ADFCS more feasible for current quantum devices in comparison to the FCS algorithm.

For example, we numerically demonstrate that ADFCS with a depth of $d^* = 3$ achieves comparable estimation precision to the FCS method when estimating the expectation value of the Kitaev chain Hamiltonian for $n = 10$ qubits. Additionally, we evaluate the ADFCS method by analyzing the estimation error for several k-local Majorana strings with varying interaction distances. The numerical results indicate that adaptively selecting a relatively shallow depth can achieve a sample complexity similar to that of FCS for most k-local Majorana strings.

The paper is organized as follows. In Sec. II, we introduce basic notations and the FCS protocol. We introduce the ADFCS algorithm in Sec. III A and represent the sample complexity in ADFCS with a tensor network contraction in Sec.III B. Sec. III C relates the sample complexity with circuit depth for two-local Majorana string and then promotes the results to k-local Majorana string for constant k in Sec. III D. We test the performance of ADFCS on several typical Majorana strings and the Kiteav chain Hamiltonian in Sec. IV. Finally, we conclude in Sec. V.

II. PRELIMINARY

Notations. A non-zero linear operator $|A\rangle\rangle$ can be vectorized as $|A\rangle\rangle := \frac{A}{\sqrt{\text{Tr}(A^\dagger A)}}$ where the normalization ensures that it is properly scaled. Specifically, for the Majorana string γ_S, the vectorized form is $|\gamma_S\rangle\rangle := \frac{\gamma_S}{\sqrt{2^n}}$, where n is the number of qubits. Moreover, the operator A can be represented by the Pauli basis, which is known as the Pauli-transfer matrix (PTM) representation, and we show further details of PTM in Appendix A. The inner product between the vectorized formation of two operators A, B is defined as $\langle\langle A|B\rangle\rangle := \frac{\text{Tr}\left(A^\dagger B\right)}{\sqrt{\text{Tr}(A^\dagger A)\text{Tr}(B^\dagger B)}}$. The operation of superoperator $\mathcal{E}$ can be denoted as $\mathcal{E}|A\rangle\rangle := \frac{\mathcal{E}(A)}{\sqrt{\text{Tr}(A^\dagger A)}}$.

Majorana operators and matchgate circuits. The Majorana operators can be defined as

$$\gamma_{2j-1} := a_j + a_j^\dagger, \quad \gamma_{2j} := -\mathrm{i}\left(a_j - a_j^\dagger\right), \tag{1}$$

where $a_j, a_j^\dagger$ are the annihilation and creation operators for the j-th site respectively. Observables in fermionic systems can be expressed as the linear combination of the products of Majorana operators [33]

$$\gamma_S := \gamma_{i_1}\gamma_{i_2}\cdots\gamma_{i_{|S|}}, \tag{2}$$

where the cardinality $|S| = \#\{i \mid i \in S\}$, $i_1 < i_2 < \cdots < i_{|S|}$, and $S = \{i_1, i_2, \cdots, i_{|S|}\}$. Especially, we set $\gamma_\emptyset$ be the identity operator $\mathbb{1}$ when S is the empty set $\emptyset$. For simplicity, we refer to a Majorana string γ_S with $|S| = k$ as a *k-local Majorana string* throughout this manuscript. Let $d_{\text{int}}(S)$ denote the interaction distance of the Majorana string γ_S, defined as

$$d_{\text{int}}(S) := \max\{\, |i_{j+1} - i_j| \mid i_j \in S,\, j \in [2n-1] \,\}. \tag{3}$$

The interaction distance of a fermionic operator $H = \sum_{S\in\mathcal{S}} \alpha_S\gamma_S$ is defined as $d_{\text{int}}(H) = \max_{S\in\mathcal{S}} d_{\text{int}}(S)$. A Majorana operator can be represented in Pauli formation as $\gamma_{2j-1} = \left(\prod_{i=1}^{j-1} Z_i\right) X_j$, $\gamma_{2j} = \left(\prod_{i=1}^{j-1} Z_i\right) Y_j$ for any $j \in [n]$ via Jordan-Wigner transformation.

Except for the standard Majorana operators in Eq. (1), there are different bases to express the fermionic Hamiltonian. Different bases can be obtained by the orthogonal transformation of the standard Majorana operators $\tilde{\gamma}_\mu = \sum_{\nu=1}^{2n} Q_{\mu\nu}\gamma_\nu$, where Q is a real orthogonal matrix, $Q \in O(2n)$. The different sets of bases $\{\tilde{\gamma}_\mu\}$ are also called the Majorana operators because they satisfy the same anti-commutation relation $\{\tilde{\gamma}_\nu, \tilde{\gamma}_\mu\} = 2\delta_{\mu\nu}$. The orthogonal transformations of Majorana operators can be represented by unitaries

$$U_Q^\dagger \gamma_\mu U_Q = \sum_{\nu=1}^{2n} Q_{\mu\nu}\gamma_\nu = \tilde{\gamma}_\mu, \tag{4}$$

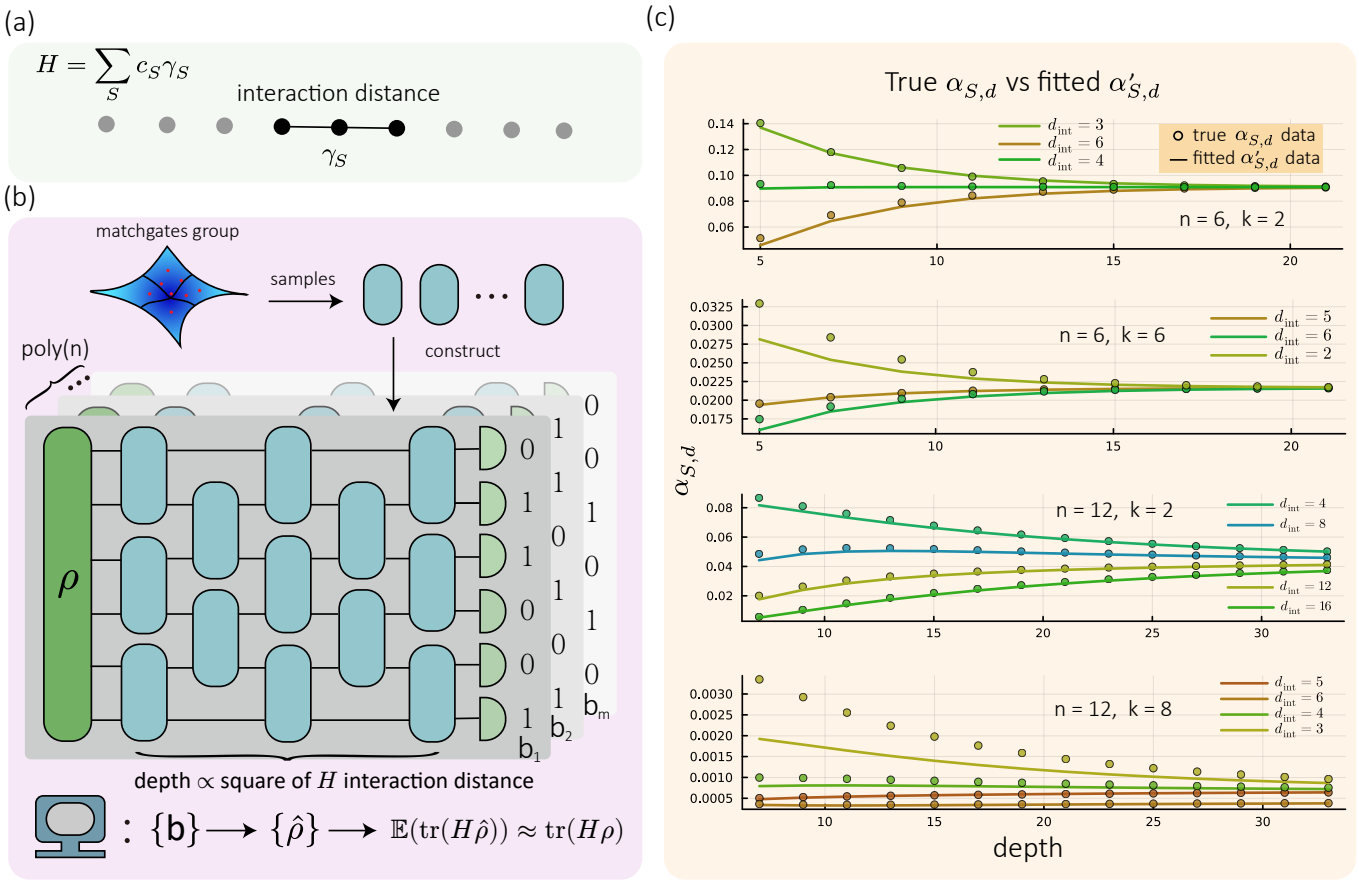

FIG. 1: Illustration of Adaptive-Depth Fermionic Classical Shadow (ADFCS). (a) The interaction distance of the observable H. The Majorana operator γ_S in H can be interpreted as the interaction between particles. The interaction distance $d_{\mathrm{int}}(H)$ is defined as the maximum interaction distance of each operator γ_S in H. (b) Sketch of the ADFCS protocol. Unitary gates are independently sampled from the group of two-qubit matchgates within a brickwork architecture. The measured bitstrings b are processed on a classical computer to generate the classical representation of ρ, and $\mathrm{Tr}(H\rho)$ can be estimated using the generated classical estimator $\hat{\rho}$. The depth of the random circuit is determined by the fermionic Hamiltonian $H = \sum c_S \gamma_S$. (c) Illustration of $\alpha'_{S,d}$ and $\alpha_{S,d}$ with the increase of depth d for different number of qubits n and Majorana strings γ_S.

where the unitaries U_Q are called fermionic Gaussian unitaries. Followed by Eq. (4), the fermionic Gaussian unitary preserves the cardinality $|S|$ of γ_S, which can be expressed as $U_Q^\dagger \gamma_S U_Q = \sum_{S' \in \binom{[2n]}{|S|}} \det\left(Q|_{S,S'}\right) \gamma_{S'}$. The set $\binom{[2n]}{|S|}$ represents the collection of all subsets of $\{1, 2, \ldots, 2n\}$ that contain exactly $|S|$ elements, and the matrix $Q|_{S,S'}$ is obtained from the matrix Q by selecting the rows indexed by the set S and the columns indexed by the set S'.

Matchgate circuits are the quantum circuit representation of fermionic Gaussian unitaries [15]. The collection of all n-qubit matchgate circuits constitutes the matchgate group $\mathbb{M}_n$. This group is generated by rotations of the form $\exp\left(\mathrm{i}\theta X_\mu X_{\mu+1}\right), \exp\left(\mathrm{i}\theta Z_\nu\right)$ and X_η, where θ is a real parameter, $\nu, \eta \in [n]$, $\mu \in [n-1]$. Notably, operations within the matchgate group can be efficiently simulated on a classical computer. This efficiency arises because the action of a matchgate circuit U_Q corresponds to Givens rotations associated with an orthogonal matrix Q, facilitating polynomial-time classical simulation [20, 34].

We present the twirling of the matchgate group in the following lemma, as it is utilized in the proof of our main results.

Lemma 1 (The three moments of uniform distribution in $\mathbb{M}_n$, Ref. [15]). *The k-moment twirling $\mathcal{E}^{(j)}$ is defined by*

$$\mathcal{E}^{(j)}(\cdot) := \int_{U_Q \in \mathbb{M}_n} \mathrm{d}U_Q \; U_Q^{\otimes j}(\cdot)U_Q^{\dagger \otimes j}. \tag{5}$$

The first three moments are

$$\begin{aligned}\mathcal{E}^{(1)} &= |\mathbb{1}\rangle\rangle\langle\langle\mathbb{1}| \\ \mathcal{E}^{(2)} &= \sum_{k=0}^{2n}\binom{2n}{k}^{-1}\sum_{\substack{S,S'\subseteq[2n]\\|S|=|S'|=k}}|\gamma_S\rangle\rangle|\gamma_S\rangle\rangle\langle\langle\gamma_{S'}|\langle\langle\gamma_{S'}| \\ \mathcal{E}^{(3)} &= \sum_{\substack{k_1,k_2,k_3\geq 0\\k_1+k_2+k_3\leq 2n}}|\mathcal{R}\rangle\rangle\langle\langle\mathcal{R}|,\end{aligned} \tag{6}$$

where

$$\begin{aligned}|\mathcal{R}\rangle\rangle =& \binom{2n}{k_1,k_2,k_3,2n-k_1-k_2-k_3}^{-1/2} \\ &\times \sum_{\substack{A,B,C\,disjoint\\|A|=k_1,|B|=k_2,|C|=k_3}}|\gamma_A\gamma_B\rangle\rangle|\gamma_B\gamma_C\rangle\rangle|\gamma_C\gamma_A\rangle\rangle.\end{aligned} \tag{7}$$

(Fermionic) classical shadow protocol. The classical shadow (CS) process involves randomly applying a unitary U from some unitary ensemble $\mathbb{U}$ (such as the Clifford group) on a quantum state ρ, followed by measurement in computational bases, yielding outcomes $|b\rangle\rangle$ that form a classical description of ρ, known as "*classical shadow*", denoted as $|\hat{\rho}\rangle\rangle = \mathcal{M}_{\mathrm{CS}}^{-1}(\mathcal{U}^{-1}|b\rangle\rangle)$, where $\mathcal{U}$ is the PTM representation of U, and $\mathcal{M}_{\mathrm{CS}} := \mathbb{E}_{\mathcal{U}\in\mathbb{U}}\left[\mathcal{U}^\dagger\sum_b|b\rangle\rangle\langle\langle b|\mathcal{U}\right]$. By choosing $\mathbb{U}$ as Clifford group Cl_n, the classical shadow channel can be simplified to $\mathcal{M}_{\mathrm{CS}} = \Pi_0 + \frac{1}{2^n+1}\Pi_1$, where Π_0 is the projector onto the identity subspace and Π_1 is the projector onto the subspace spanned by all Pauli bases except identity [11, 35]. This simple representation allows efficient construction of the classical shadow $\hat{\rho}$.

In the framework of FCS, the shadow channel $\mathcal{M}_{\mathrm{FCS}} := \mathbb{E}_{Q\in O(2n)}\left[\mathcal{U}_Q^\dagger\sum_b|b\rangle\rangle\langle\langle b|\mathcal{U}_Q\right]$ is not invertible across the entire Hilbert space. Its invertibility is constrained to a subspace spanned by even operators, denoted as $\Gamma_{\mathrm{even}} := \mathrm{span}\{\gamma_S \mid |S| = 2j, j = 0, 1, 2, \cdots, n\}$. For set S with odd cardinality, the channel $\mathcal{M}_{\mathrm{FCS}}(\gamma_S) = 0$, rendering these components inaccessible.

As a result, FCS is limited to recovering expectation values of observables that reside within the Γ_{even} subspace. However, this restriction is sufficient for capturing physical observables, as they are typically even operators due to the conservation of fermionic parity [36]. Unless otherwise specified, all discussions and calculations are assumed to take place within the Γ_{even}.

III. ADAPTIVE-DEPTH FERMIONIC CLASSICAL SHADOWS

Here, we consider the ADFCS by selecting the unitary ensemble as d-depth local matchgates with brickwork architecture, as shown in Fig. 1(b), which is widely applied in superconducting quantum devices [21]. It has been shown that certain observables cannot be addressed by replacing the global $\mathrm{Cl}_n \cap \mathbb{M}_n$ group with shallow-depth local matchgate circuits [13]. However, it remains open when global elements are necessary and how to efficiently generate the expectation values of a given set of fermionic observables using the shallowest depth matchgate circuits while minimizing the number of samplings. Here, we address this question by exploring the relationship between the number of required samples and the depth of the matchgate circuit for some specific set of fermionic observables using the brickwork architecture. Our approach introduces a d-depth ADFCS channel to estimate the expectation value of a fermionic observable H. The estimation of the expectation value is divided into a series of estimations of Majorana observables $\{\gamma_S\}$. The optimal depth order is determined by the maximum interaction distance of the set $\{\gamma_S\}$.

A. Shadow channel analysis in ADFCS

For simplicity, we utilize U_{Q_d} to denote a d-depth matchgate circuit with brickwork structure, and $\mathbb{U}_{Q_d}$ to denote the set of all d-depth matchgate circuit throughout this manuscript. We denote $\mathcal{M}_d$ as the d-depth ADFCS shadow channel, which maps a quantum state ρ to

$$\mathcal{M}_d(\rho) := \mathop{\mathbb{E}}_{U\in\mathbb{U}_{Q_d}}\left[\sum_{b\in\{0,1\}^n}\langle b|U_{Q_d}\rho U_{Q_d}^\dagger|b\rangle U_{Q_d}^\dagger|b\rangle\langle b|U_{Q_d}\right]. \tag{8}$$

Due to the expectation property of the subset $\mathbb{U}_{Q_d}$, the Majorana operator remains invariant under the action of $\mathcal{M}_d$ up to a scaling factor $\alpha_{S,d}$, i.e.,

$$\mathcal{M}_d(\gamma_S) = \alpha_{S,d}\gamma_S, \tag{9}$$

where $\alpha_{S,d} := \int \mathrm{d}U_{Q_d}\left|\langle\mathbf{0}|U_{Q_d}\gamma_S U_{Q_d}^\dagger|\mathbf{0}\rangle\right|^2$. The proof is shown in Appendix B.

First, we show that the ADFCS can unbiasedly rebuild the state ρ, thereby providing an unbiased estimation of the expectation value. Directly follows from the linearity of the shadow channel $\mathcal{M}_d$, we have

$$\begin{aligned}&\mathop{\mathbb{E}}_{U_{Q_d},b}(\mathcal{M}_d^{-1}(U_{Q_d}^\dagger|b\rangle\langle b|U_{Q_d})) &(10)\\ =&\mathcal{M}_d^{-1}(\mathbb{E}(U_{Q_d}^\dagger|b\rangle\langle b|U_{Q_d})) &(11)\\ =&\rho &(12)\end{aligned}$$

when $\alpha_{S,d}$ is non-zero.

Eq. (12) demonstrates that the ADFCS protocol provides an unbiased estimation. We now analyze the required sample complexity to achieve high precision. For any observable γ_S with respect to the average of quantum states ρ, the variance of the ADFCS estimator $v = \mathrm{Tr}(\hat{\rho}\gamma_S)$ is bounded as follows:

$$\mathrm{Var}[v] \leq \frac{1}{\alpha_{S,d}}. \tag{13}$$

The detailed derivation of Eq. (13) is provided in Appendix C. Using this result and applying Chebyshev's inequality, the estimation error $|v - \mathrm{Tr}(\rho\gamma_S)|$ can be bounded to ε using $\mathcal{O}(\frac{1}{\alpha_{S,d}\varepsilon^2})$ copies of the quantum states with high success probability. Numerical results demonstrate that the variance is stable across various quantum states. In the following sections, we will present the calculation for $\alpha_{S,d}$, along with its lower bound.

B. Tensor network approach to variance bound

By Eq. (13), bounding the variance requires calculating $\alpha_{S,d}$. Here, we demonstrate that $\alpha_{S,d}$ can be represented as a tensor network and computed through contraction. Using the PTM representation, $\alpha_{S,d}$ can be expressed as

$$\alpha_{S,d} = \langle\langle \mathbf{0}, \mathbf{0}| \int \mathrm{d}\mathcal{U}_{Q_d} \mathcal{U}_{Q_d}^{\otimes 2} |\gamma_S, \gamma_S\rangle\rangle, \tag{14}$$

where $\mathcal{U}_{Q_d}$ is the superoperator of U_{Q_d}, $\mathcal{U}_{Q_d}|\gamma_S\rangle\rangle = U_{Q_d}\gamma_S U_{Q_d}^\dagger$. Consequently, the integration over $\mathcal{U}_{Q_d}$ can be broken down into a product of a series of integrations over the independent 2-qubit matchgates. By Lemma 1, we can represent the integration over each 2-qubit matchgate as a fourth-order tensor $\mathcal{T}$ with indices $\sigma_1, \sigma_2, \sigma_3, \sigma_4$. The explicit form of this tensor is given by

$$\mathcal{T}^{\sigma_1\sigma_2}_{\sigma_3\sigma_4} := \langle\langle \sigma_1, \sigma_2|^{\otimes 2} \int_{Q\sim O(4)} \mathrm{d}\mathcal{U}_Q \mathcal{U}_Q^{\otimes 2} |\sigma_3, \sigma_4\rangle\rangle^{\otimes 2}, \tag{15}$$

where the indices $\sigma_1, \sigma_2, \sigma_3, \sigma_4$ of tensor $\mathcal{T}$ represent the Pauli operators. The tensor $\mathcal{T}$ is the integration of one blue random gate in Fig. 1. By connecting these tensors $\mathcal{T}$ in the same brickwork architecture as U_{Q_d}, the integration over the superoperator in Eq. (14) can be transformed into a tensor network. The transformation details are shown in Appendix D.

The value of $\alpha_{S,d}$ can be calculated by contracting the corresponding brickwork tensor network, which is shown in Fig. 2(a). Specifically, the brickwork tensor network, denoted as $\mathcal{C}$, is contracted with $\langle\langle \mathbf{0}, \mathbf{0}|$ and $|\gamma_S, \gamma_S\rangle\rangle$ in the PTM representation to calculate $\alpha_{S,d}$

$$\alpha_{S,d} = \langle\langle \mathbf{0}, \mathbf{0}|\mathcal{C}|\gamma_S, \gamma_S\rangle\rangle. \tag{16}$$

Following the proof of Lemma 5 in Ref. [24], the tensor network $\mathcal{C}$ can be represented by a matrix product operator with bond dimension $2^{\mathcal{O}(d)}$. It suggests that calculating $\alpha_{S,d}$ by tensor network contraction is efficient only when the depth d is shallow.

C. Adaptive depth for two-local Majorana strings

Here, we start by determining the optimal depth order for the random matchgate circuit U_{Q_d}, such that the estimation of a set of 2-local Majorana strings $\{\gamma_S | \, |S| = 2\}$ requires the same sample complexity compared to the full matchgate group $\mathbb{M}_n$. Notably, for specific sets of Majorana strings $\{\gamma_S\}$, the optimized number of measurements can be significantly improved compared to FCS when using a smaller d. As an instance, suppose we need to estimate the expectation of $\gamma_i\gamma_{i+1}$. The random measurement in FCS actually shuffles the $\gamma_i\gamma_{i+1}$ to any $\gamma_j\gamma_k$ uniformly. However, a matchgate circuit with $d = 2$ will only slightly perturb the $\gamma_i\gamma_{i+1}$ to the nearby operators $\{\gamma_j\gamma_k \mid i-2 \le j \le i+2, i-1 \le k \le i+3\}$. A smaller sample space allows it to approach its theoretical mean with fewer samples compared to the FCS method.

We will investigate how the sample complexity of the quantum state changes as the depth of the matchgate circuits with brickwork structures increases. To determine the required depth of a random matchgate circuit for efficient measurement of a specific set of 2-local Majorana strings $\{\gamma_S\}$, we derive an expression for $\alpha_{S,d}$ and identify the optimal depth d^* such that $\alpha_{S,d^*} = \frac{1}{\mathcal{O}(\mathrm{poly}(n))}$. By restricting the input state of the whole tensor network $\mathcal{C}$ to the subspace Γ_2, we can simplify the tensor contraction into a polynomial space. This isomorphism introduces more refined structures and allows us to analyze the system more effectively.

We will focus on random matchgate circuits characterized by an even number of qubits and an odd circuit depth. For the random matchgate circuits with this structure, the contraction of $\mathcal{C}$ can be represented within the space of quadratic polynomials with $\frac{n}{2}$ variables. For the circuits with even circuit depth, the contraction can be analyzed using a similar method. Denote the quadratic polynomial representation space as $\mathcal{P}_{\frac{n}{2}}$, the contraction of $\mathcal{C}$ can be described by the random walk with a simple pattern in space $\mathcal{P}_{\frac{n}{2}}$.

To represent this random walk, we use the transition process $\mathcal{B}$ to denote a pair of successive gate layers starting from an odd layer (see Fig. 2(a)),

$$\mathcal{B}|\gamma_S, \gamma_S\rangle\rangle = \sum_{S':|S'|=|S|} \mathrm{Prob}(\gamma_{S'}|\gamma_S)|\gamma_{S'}, \gamma_{S'}\rangle\rangle, \tag{17}$$

The contraction of $\mathcal{C}$ can be understood as the repeated application of $\mathcal{B}$ to the state $|\gamma_S, \gamma_S\rangle\rangle$. As previously mentioned, we focus on the circuit with odd depth. Then, the entire tensor network can be expressed as

$$\mathcal{C} = \mathcal{B}^{\lfloor d/2 \rfloor} \mathcal{T}_{\mathrm{init}}, \tag{18}$$

where $\mathcal{T}_{\mathrm{init}} = \mathcal{T}^{\otimes \frac{n}{2}}$ (and the circuit can be expressed as $\mathcal{C} = \mathcal{B}^{d/2}$ if the depth is an even number). Each $\mathcal{B}$ corresponds to a single transition step in a random walk. Therefore, the entire tensor network $\mathcal{C}$ represents a random walk starting from the site corresponds to γ_S and taking the transition $\lfloor \frac{d}{2} \rfloor$ steps, which is shown in Fig. 2(c). The details of mapping the tensor contraction of $\alpha_{S,d}$ to the random walk in $\mathcal{P}_{\frac{n}{2}}$ is shown in Appendix E.

We observe that the random walk follows the pattern of a symmetry lazy random walk (SLRW) [37, 38] almost everywhere within the polynomial space $\mathcal{P}_{\frac{n}{2}}$. SLRW is a

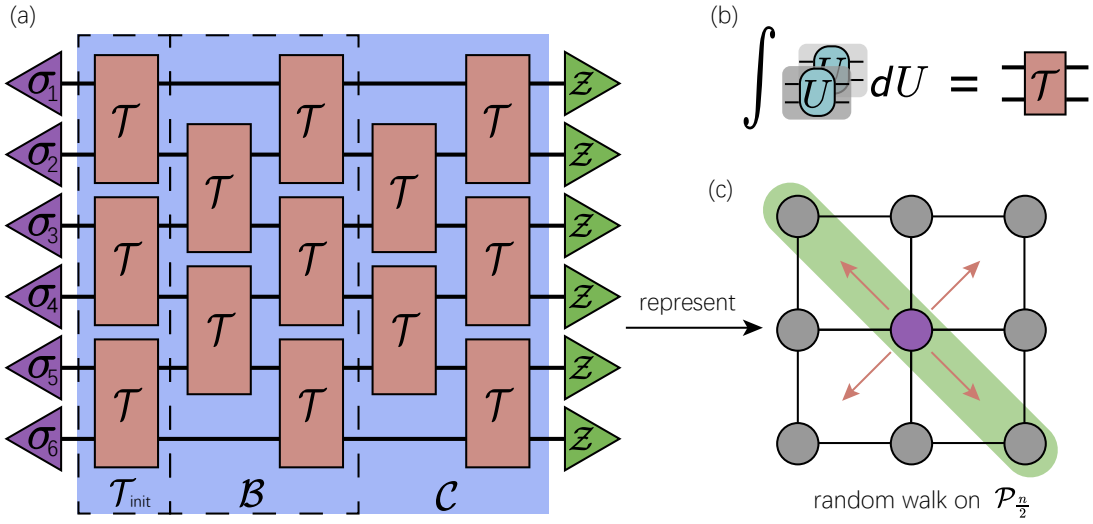

FIG. 2: Representation of the tensor contraction of $\mathcal{C}$ as a random walk on the polynomial space $\mathcal{P}_{\frac{n}{2}}$. (a) The tensor network is used to compute $\alpha_{S,d}$. The purple triangles represent Pauli operators corresponding to γ_S via the Jordan-Wigner transformation, while the green triangles, denoted as $\mathcal{Z}$, correspond to the supervector $\frac{1}{2}(|\mathbb{1},\mathbb{1}\rangle\rangle + |Z,Z\rangle\rangle)$. (b) The definition of $\mathcal{T}$ in Eq. (15). (c) The contraction of $\mathcal{C}$ onto the polynomial space $\mathcal{P}_{\frac{n}{2}}$. Transitioning the state $|\gamma_S,\gamma_S\rangle\rangle$ and contracting it with $\mathcal{Z}$ is equivalent to summing the probabilities over the diagonal sites in a 2D random walk.

stochastic process in which the walker has a probability of staying in the same position at each step and equal probabilities of moving to neighboring positions. Firstly, we consider the random walk transition $\mathcal{B}$ across the subspace Γ_2 adheres to the SLRW

$$\mathcal{L}_{\Gamma_2}|\gamma_S,\gamma_S\rangle\rangle = \sum_{S':|S'|=|S|} \mathrm{Prob}_L(\gamma_{S'}|\gamma_S)|\gamma_{S'},\gamma_{S'}\rangle\rangle, \quad (19)$$

where $\mathcal{L}_{\Gamma_2}$ is the transition operator in SLRW, and the concrete form of $\mathcal{L}_{\Gamma_2}$ is shown in Appendix E 2, Eq. (E19). We replace the transition operator $\mathcal{B}$ with the SLRW transition operator $\mathcal{L}_{\Gamma_2}$ in $\mathcal{C}$ and use the transition $\mathcal{L}_{\Gamma_2}$ to calculate the tensor network contraction

$$\alpha^L_{S,d} = \langle\langle \mathbf{0},\mathbf{0}|\mathcal{L}^{\lfloor\frac{d}{2}\rfloor}_{\Gamma_2}\mathcal{T}_{\mathrm{init}}|\gamma_S,\gamma_S\rangle\rangle. \quad (20)$$

As we have shown in Table II of Appendix E, the transition result of $\mathcal{L}_{\Gamma_2}$ equals the results $\mathcal{B}$ for most states in Γ_2, this indicates that the variable $\alpha^L_{S,d}$ likely constitutes the dominant contribution to $\alpha_{S,d}$. Additionally, numerical fitting further confirms that $\alpha_{S,d}$ is primarily governed by $\alpha^L_{S,d}$, as shown in Fig. 1 (b).

There is a known analytical propagation equation for the SLRW [37]. By applying this propagation equation and making certain approximations, the $\alpha_{S,d}$ can ultimately be expressed as a Poisson summation

$$\alpha^L_{S,d} = \frac{1}{3\sqrt{\pi(d-1)}}\sum_{k=-\infty}^{\infty}\left(e^{-\frac{(kn+a)^2}{d-1}} + e^{-\frac{(kn+b)^2}{d-1}}\right) + \mathcal{O}(e^{-\pi^2 d}). \quad (21)$$

In Eq. (21), we denote the Majorana observable γ_S with $|S| = 2$ as $\gamma_i\gamma_j$, the variable a, b are defined by $a := |\lfloor\frac{i-1}{4}\rfloor - \lfloor\frac{j-1}{4}\rfloor|$, and $b := \lfloor\frac{i-1}{4}\rfloor + \lfloor\frac{j-1}{4}\rfloor + 1$. We leave the detailed proof of Eq. (21) to Appendix F.

We aim to estimate the order of $\alpha_{S,d}$ by $\alpha^L_{S,d}$, which can be achieved by bounding the ratio $\alpha_{S,d}/\alpha^L_{S,d}$ to a constant value. To bound the ratio, we introduce an auxiliary function

$$\Delta(S,S',d) = \langle\langle\gamma_{S'},\gamma_{S'}|\mathcal{B}^{\lfloor\frac{d}{2}\rfloor}\mathcal{T}_{\mathrm{init}} - \mathcal{L}^{\lfloor\frac{d}{2}\rfloor}_{\Gamma_2}\mathcal{T}_{\mathrm{init}}|\gamma_S,\gamma_S\rangle\rangle, \quad (22)$$

where $S' \in \Gamma_2$. Recall that the operator $\gamma_{S'}$ is defined as $\gamma_{S'} = \gamma_u\gamma_v$ where $S' = \{u,v\}$. In numerical experiments, we observe that the term $\Delta(S,S',d)$ is negative if and only if the element u is close to v for $S' = \{u,v\}$ and any S,d, as shown in Fig. 8 of Appendix G. Based on this finding, we show that the ratio $\alpha_{S,d}/\alpha^L_{S,d}$ can be bounded by a constant value. The concrete description for bounding the ratio $\alpha_{S,d}/\alpha^L_{S,d}$ is provided in Appendix G.

The relation between $\alpha^L_{S,d}$ and $\alpha_{S,d}$, named $\alpha_{S,d} \geq c\alpha^L_{S,d}$ for positive constant c, indicated that the order of $\alpha^L_{S,d}$ consistent with the order of $\alpha_{S,d}$. Here, we propose the adaptive depth d^* of a random matchgate circuit by analyzing the order of $\alpha^L_{S,d}$. By Eq. (21), for $a = \mathcal{O}(\log(n))$ and the measurement depth $d^* = \mathcal{O}(\log n)$ can yield a polynomially small $\alpha_{S,d^*} = \Omega\left(\frac{1}{n}\right)$ up to a log factor, we postpone the proof in Appendix H. When $a = \omega(\log(n))$, the remainder error term $\mathcal{O}(e^{-\pi^2 d})$ in Eq. (21) scales polynomially small. Thus, we adaptively select the depth d based on the first term of $\alpha^L_{S,d}$, which

is decided by the interaction distance $d_{\text{int}} = |i-j|$,

$$d^* = \Theta\left(\max\left\{\frac{d_{\text{int}}^2}{\log(n)},\ d_{\text{int}}\right\}\right). \tag{23}$$

We show that the $\alpha_{S,d}^L$ scales as $/\mathcal{O}(1\text{poly}(n))$ when the depth is selected as d^* in Appendix F Lemma 5. Combined with the relationship between $\alpha_{S,d}^L$ and $\alpha_{S,d}$, it suggests that the sample complexity scales polynomially with the adaptively selected depth d^*.

D. Adaptive depth for general k-local Majorana strings

Here, we focus on extending adaptive depth to general k-local Majorana strings for constant k. Fermionic observables generated by k-local Majorana strings for constant k play a critical role in various quantum models across physics and chemistry. These operators are essential in describing physical observables such as interaction terms, electron correlation, and pairing mechanisms. They appear in models like quantum chemistry Hamiltonians, generalized Hubbard models, spin chain models, etc [1–6].

The required circuit depth depends on the interaction distance d_{int} of γ_S. Recall Eq. (2) that the elements in S are a monotonically increasing sequence. Thus, the d_{int} can be interpreted as the maximum distance between adjacent elements in S. We prove that a random measurement circuit $\mathcal{U}_{Q_d}$ with $d = \Theta(\log n)$ is sufficient to make $\alpha_{S,d}$ as large as $1/\mathcal{O}(\text{poly}(n))$ if $d_{\text{int}} = \mathcal{O}(\log n)$ and k is a constant. From Eq. (16) and Eq. (17), we conclude that the value of $\alpha_{S,d}$ is the sum of probabilities associated with specific sites after the random walk. When the distance of the near neighborhood $i_{2j-1}, i_{2j} \in S$ logarithmically small $i_{2j} - i_{2j-1} = \mathcal{O}(\log n)$, a logarithmically transition steps can traverse from corresponding $|\gamma_S, \gamma_S\rangle\rangle$ to specific sites. Due to Eq. (17), each step introduces a constant probability factor. Thus, the probability of reaching specific sites is $\frac{1}{\mathcal{O}(n^{k/2})}$ up to a log factor after logarithmic steps random walk. We put the proof details in Appendix H.

We propose a general formula for approximating $\alpha_{S,d}$. The proposed formula considers the random walk for computing $\alpha_{S,d}$ as the several independent $k = 2$ random walks. Any pair $i, j \in S$ are treated as an independent random walk starting from corresponding $\gamma_i\gamma_j$. After the overall random walk, the probability of being at a specific site equals the product of the probabilities of each 2-local $\gamma_{S'}$ at that site. As a result, the sum of probabilities at these specific sites can be expressed as a production $\prod \alpha_{\{i,j\},d}$. Therefore, we consider the overall random walk as the superposition of all such production

$$\alpha'_{S,d} = \frac{1}{(k-1)!!}\left(\frac{3n}{2}\right)^{\frac{k}{2}} \frac{\binom{n}{k/2}}{\binom{2n}{k}} \sum_{\Lambda\in\text{Par}(S)} \prod_{(i,j)\in\Lambda} \alpha_{\{i,j\},d}^L, \tag{24}$$

where $\text{Par}(S)$ is the set whose elements Λ are sets representing pairwise partitions of S. For example, let $S = \{1,2,3,4\}$, then $\Lambda = \{(1,2),(3,4)\}$ is a pairwise partitions of S.

Numerical experiments indicate that the proposed expression $\alpha'_{S,d}$ closely approximates $\alpha_{S,d}$ for depths $d > 2\log(n)$. When the interaction distance $d_{\text{int}}(S) = \mathcal{O}(\log n)$, the optimal depth for random matchgate circuits is $\mathcal{O}(\log n)$, making them shallow and well-suited for near-term quantum devices. Given this compatibility, our analysis focuses on bounding $\alpha_{S,d}$ with $\alpha'_{S,d}$ in the regime where $d = \omega(\log n)$. Therefore, it can be concluded that $\alpha'_{S,d}$ provides a good approximation of $\alpha_{S,d}$. Fig. 1(b) shows the results of comparison between $\alpha'_{S,d}$ and $\alpha_{S,d}$. The curve of $\alpha'_{S,d}$ is very close to the $\alpha_{S,d}$ when $d > 2\log(n)$, which suggests that the $\alpha'_{S,d}$ is a good approximation of $\alpha_{S,d}$ as well.

We adaptively select the depth based on the interaction distance d_{int} of a fermionic Hamiltonian H, where $d_{\text{int}}(H)$ is the maximum value of $d_{\text{int}}(S)$ for terms γ_S in H. Similar to the case with $|S| = 2$, we adaptively select the depth d^* as

$$d^* = \Theta\left(\max\left\{\frac{d_{\text{int}}(S)^2}{\log(n)}, d_{\text{int}}(S)\right\}\right). \tag{25}$$

Such d^* ensures that existing a term in Eq. (24) scales polynomially, thereby guaranteeing the overall $\alpha'_{S,d}$ also scales polynomially.

IV. NUMERICAL EXPERIMENT

Here, we provide numerical evidence demonstrating the efficiency of the ADFCS protocol. First, we compare the performance of ADFCS with FCS across various circuit depths and observables γ_S. For each experiment, a random 10-qubit quantum state ρ is chosen, followed by a d-depth random matchgate circuit with the brickwork structure and measurement on the computational basis. We enumerate depth d in $\{5, 9, 15, 19, 23\}$. The estimation error with increasing numbers of measurements for ADFCS with different depth d and FCS is shown in Fig. 3. We estimate the error for the estimations of $\text{Tr}(\gamma_S\rho)$ for $k = |S| \in \{2, 4, 6\}$ as the number of samples increases. Each subfigure corresponds to a different set S, chosen based on varying $d_{\text{int}}(S)$. The error is estimated as $\sqrt{\frac{1}{R}\sum_{i=1}^{R}(\text{Tr}(\gamma_S\hat{\rho}_i) - \text{Tr}(\gamma_S\rho))^2}$, where $\hat{\rho}_i$ is generated from the i-th measurement, and R is set to 64.

The required depth of the random matchgate circuit for a specific observable γ_S depends on the value of $\alpha_{S,d}$, thereby relying on the interaction distance $d_{\text{int}}(S)$. Shallower circuits tend to perform better when the interaction distance is small, whereas larger interaction distances necessitate deeper circuits. For instance, when $d_{\text{int}}(S) \in \{3, 4\}$, random matchgate circuits with depth $d = 5$ provide good estimations of the expectation value. However,

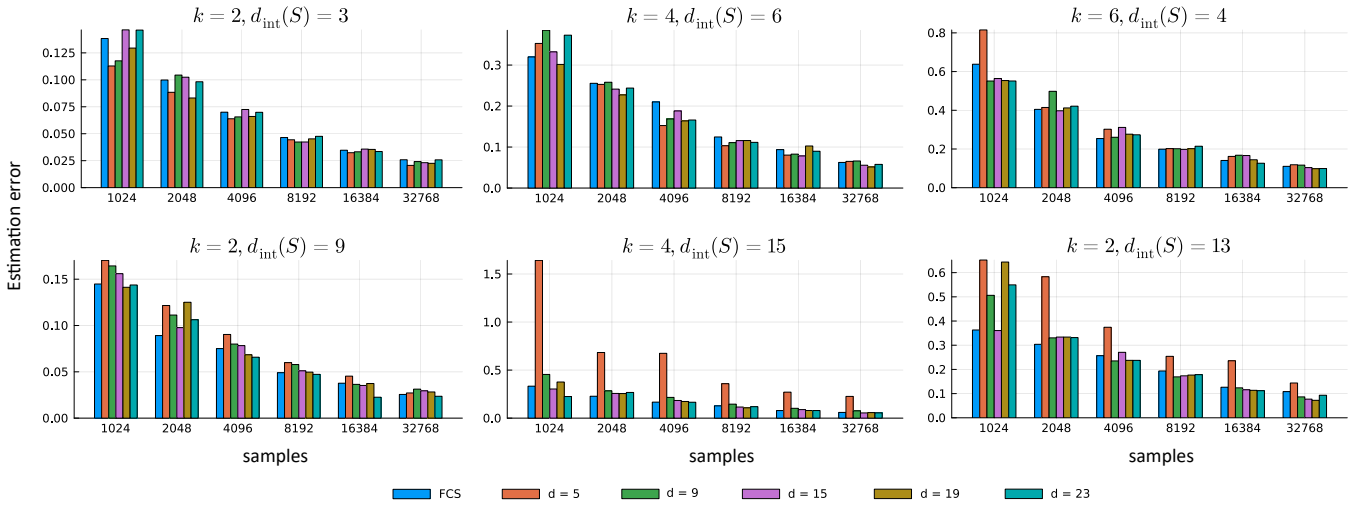

FIG. 3: Estimation errors with increasing numbers of measurements for FCS and ADFCS protocols at different depths d and interaction distance d_{int}. Each experiment uses a randomly generated 10-qubit quantum state.

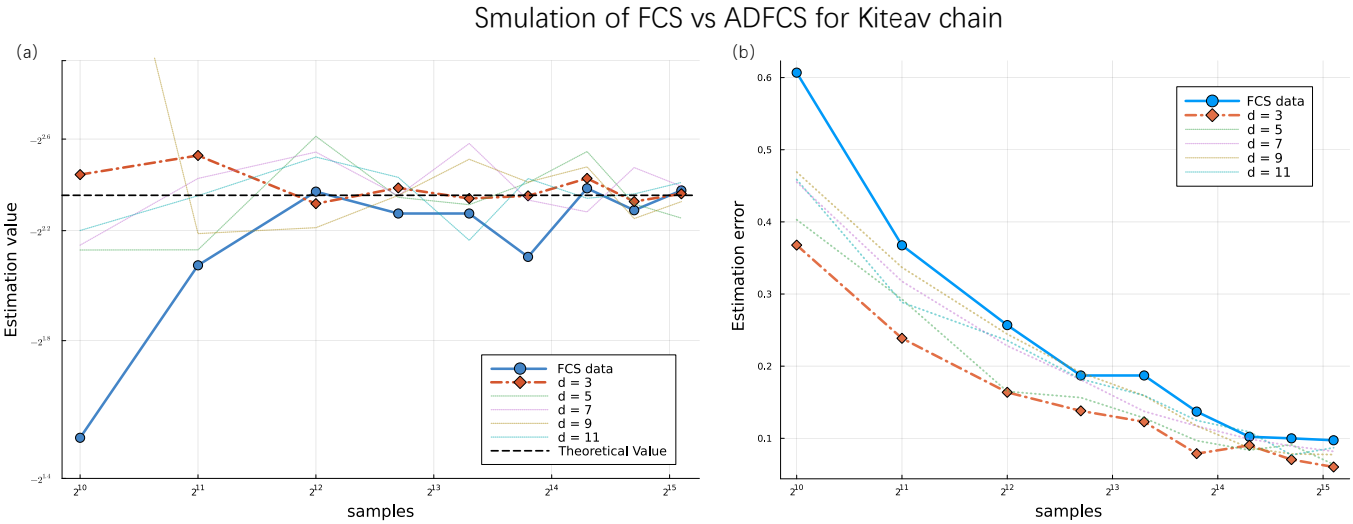

FIG. 4: Application of ADFCS to the Kitaev chain Hamiltonian H_K. (a) The estimation generated from FCS and ADFCS with varying circuit depths. (b) The error between the estimation and the expectation value.

for larger interaction distances, such as $d_{\text{int}}(S) = 13$ or 15, a depth of $d = 5$ is insufficient to ensure accurate results. In such cases, circuits with a depth of $d \geq 9$ are necessary to achieve reliable estimations. By selecting an appropriate circuit depth, accurate estimations can be obtained with a relatively small number of samples, ensuring both efficiency and precision. In each subfigure of Fig. 3, we use different random states for various choices of S. The numerical results demonstrate that ADFCS is robust to random states, despite the definition of $\alpha_{S,d}$ being based on the average over states ρ.

To further test the performance of ADFCS, we apply the method of estimating the expectation of the Kiteav chain Hamiltonian. The Kitaev chain Hamiltonian is a one-dimensional model that describes a topological superconductor featuring Majorana fermions at its ends [39]. The Kiteav chain Hamiltonian is given by

$$H_K = -\frac{\mathrm{i}\mu}{2}\sum_{j=1}^{n}\gamma_{2j-1}\gamma_{2j} + \frac{\mathrm{i}}{2}\sum_{j=1}^{n-1}\left(\omega_+\gamma_{2j-1}\gamma_{2j+2} - \omega_-\gamma_{2j}\gamma_{2j+1}\right), \tag{26}$$

where μ is the chemical potential, $\omega_\pm = |\Delta| \pm t$, both Δ and $\mathcal{T}$ are certain energy gaps. We initialize a random state for 10-qubit, set these parameters as $\mu = 2$, $\Delta = 1$, and $t = 0.4$. The results are shown in Fig. 4. Since the maximum interaction distance of H_K is $d_{\text{int}}(H_K) = 3$, a random circuit with a depth of $d = 3$ yields an acceptable value of $\alpha_{S,d}$. This results in comparable or even improved estimation errors compared to the FCS

protocol, while requiring significantly less circuit depth.

V. CONCLUSION AND DISCUSSION

We propose an adaptive depth fermionic classical shadow (ADFCS) protocol to reduce the heavy circuit depth associated with random matchgate circuits in fermionic classical shadow (FCS) protocol. Using a tensor network approach, we calculate the variance for any d-depth ADFCS protocol, enabling us to determine the required depth d to ensure efficient sampling.

Furthermore, we theoretically analyze the explicit relationship between the variance and the depth d of the random matchgate circuit. Specifically, under certain assumptions, we find that the optimal depth is bounded by $\mathcal{O}\left(\max\left\{d_{\text{int}}(H)^2/\log n, d_{\text{int}}(H)\right\}\right)$ where $d_{\text{int}}(H)$ is the interaction distance for the fermionic observable H. Numerical fitting results are also provided to support our theoretical findings.

We validate the correctness of our algorithm by evaluating the expectation values of several Majorana strings with respect to randomly generated quantum states ρ. The numerical results align with and support our theoretical findings. Additionally, we applied our algorithm to estimate the expectation value of a Kitaev chain Hamiltonian. Comparative numerical analysis demonstrates that our ADFCS algorithm achieves performance comparable to the FCS algorithm while requiring a significantly shallower circuit depth.

Interestingly, while the complexity of general random unitaries grows linearly with the number of layers, where each layer is defined as a block of n-layer random circuits [40], this linear growth does not appear to hold for random unitaries sampled from specific groups, such as the matchgate group. Through numerical fitting, we demonstrate that the required number of layers in our ADFCS protocol to bound the variance is asymptotically optimal. In the worst-case scenario, where $d_{\text{int}}(H) = \Theta(n)$, the ADFCS protocol requires $\mathcal{O}\left(n^2/\log n\right)$ layers of random matchgate circuits. Notably, this depth is greater than the optimal depth $\mathcal{O}(n)$ to construct general matchgate circuits [20]. This observation raises an intriguing open question about how the optimal depth grows for random circuit sampled from specific groups.

ACKNOWLEDGEMENTS

We would like to thank Dax Enshan Koh, Christian Bertoni, and Jiapei Zhuang for their helpful discussions. This work was funded by the National Natural Science Foundation of China under Grant 12405014.

Appendix A: Introduction to Pauli-transfer matrix representation

By employing the Jordan-Wigner transformation, we can express γ_S in terms of Pauli operators. The Pauli-transfer matrix (PTM) representation uses these Pauli operators $\{\sigma_i\}_{i=1}^{2^n}$ as a basis, where $\sigma_i = P_i/\sqrt{2^n}$ is the normalized Pauli operator, allowing us to denote the non-zero linear operators A as a 4^n-length vector $|A\rangle\rangle$ with the j-th entry being

$$A_j = \text{Tr}(A\sigma_j). \tag{A1}$$

In this representation, a channel of operators can be expressed as a matrix Λ with the (a,b)-th element being

$$\Lambda(a,b) = \text{Tr}(\sigma_b \Lambda(\sigma_a)). \tag{A2}$$

Using this expression, we can represent the second moment of the random matchgate as a fourth-order tensor, which is shown in Appendix D.

Appendix B: Majorana operators diagonalize shadow channel

This section shows the details about diagonalizing shadow channel $\mathcal{M}_d$. Notice that the computational basis $|b\rangle$ are Gaussian states

$$|b\rangle\langle b| = \prod_{j=1}^{n} \frac{1}{2}\left(I - \mathrm{i}(-1)^{b_j}\gamma_{2j-1}\gamma_{2j}\right). \tag{B1}$$

Thus, any basis $|b\rangle\langle b|$ can be prepared from the state $|b\rangle\langle b|$ by a Gaussian unitary $U_Q \in \mathbb{M}_n$, which indicates that Pauli-X is in the matchgate group. The state $|b\rangle = |b_1 b_2 \cdots b_n\rangle$ can be denoted as $\prod X_i^{b_i}|0\rangle$. Since Pauli-X is in the matchgate group, we can absorb the $\prod X_{b_i}$ into the matchgates U_{Q_d} in the expression of shadow channel

$$\mathcal{M}_d(\gamma_S) = \int \mathrm{d}U_{Q_d} \sum_{b\in\{0,1\}^n} \langle b|U_{Q_d}\gamma_S U_{Q_d}^\dagger|b\rangle U_{Q_d}^\dagger|b\rangle\langle b|U_{Q_d} \tag{B2}$$

$$= 2^n \int \mathrm{d}U_{Q_d} \langle 0|U_{Q_d}\gamma_S U_{Q_d}^\dagger|0\rangle U_{Q_d}^\dagger|0\rangle\langle 0|U_{Q_d}. \tag{B3}$$

If S' is not equal to S and the depth d is not equal to zero, then there exists a permutation matrix Q'_d in one depth matchgate circuit such that

$$[\gamma_S, U_{Q'_d}] = 0, \quad \{\gamma_{S'}, U_{Q'_d}\} = 0. \tag{B4}$$

The orthogonal matrix Q'_d can be constructed in one depth because such U'_{Q_d} can be a Pauli operator, which involves one depth matchgate circuit. It implies

$$\frac{1}{2^n}\mathrm{Tr}\left(\gamma_{S'}\mathcal{M}_d(\gamma_S)\right) = \int \mathrm{d}U_{Q_d} \langle 0| U_{Q_d}\gamma_S U_{Q_d}^\dagger |0\rangle \langle 0| U_Q \gamma_{S'} U_{Q_d}^\dagger |0\rangle \tag{B5}$$

$$= \int \mathrm{d}U_{Q_d} \langle 0| U_{Q_d}U_{Q'_d}\gamma_S U_{Q'_d}^\dagger U_{Q_d}^\dagger |0\rangle \langle 0| U_{Q_d}U_{Q'_d}\gamma_{S'} U_{Q'_d}^\dagger U_{Q_d}^\dagger |0\rangle \tag{B6}$$

$$= -\int \mathrm{d}U_{Q_d} \langle 0| U_{Q_d}\gamma_S U_{Q_d}^\dagger |0\rangle \langle 0| U_{Q_d}\gamma_{S'} U_{Q_d}^\dagger |0\rangle . \tag{B7}$$

The result shows that $\mathrm{Tr}\left(\gamma_{S'}\mathcal{M}_d(\gamma_S)\right) = 0$ when S' is not equal to S, thereby $\mathcal{M}_d(\gamma_S) = \alpha_{s,d}\gamma_S$.

Appendix C: Bound the variance of ADFCS estimator with $\alpha_{S,d}$

The variance of the random variable $v = \mathrm{Tr}(\hat{\rho}\gamma_S)$ is analyzed by deriving an upper bound on its value. First, the variance is bounded by the expected squared magnitude of v, i.e., $\mathrm{Var}[v] \le \mathbb{E}[|v|^2]$. The expectation is then expressed as an integral over the unitary group U_{Q_d} and averaged over the state ρ

$$\mathbb{E}[|v|^2] = \int \mathrm{d}U_{Q_d}\, \mathbb{E}_\rho \Big[\sum_b \langle b|U_{Q_d}\rho U_{Q_d}^\dagger|b\rangle \times \left|\langle b|U_{Q_d}\mathcal{M}_d^{-1}(\gamma_S)U_{Q_d}^\dagger|b\rangle\right|^2 \Big]. \tag{C1}$$

Now, we start to simplify the expression. Firstly, we average out the ρ, which leads to

$$\mathbb{E}[|v|^2] = 2^{-n}\int \mathrm{d}U_{Q_d} \sum_b \left|\langle b|U_{Q_d}\mathcal{M}_d^{-1}(\gamma_S)U_{Q_d}^\dagger|b\rangle\right|^2. \tag{C2}$$

Next, we denote $|b\rangle$ as $\prod_i X_i^{b_i}|0\rangle$ and absorb the Pauli X operators into the matchgate operators. And then uses Eq. (9)

$$\mathbb{E}[|v|^2] = \frac{1}{|\alpha_{S,d}|^2}\int \langle 0|U_{Q_d}\gamma_S U_{Q_d}^\dagger|0\rangle\langle 0|U_{Q_d}\gamma_S^\dagger U_{Q_d}^\dagger|0\rangle \tag{C3}$$

$$= \frac{1}{\alpha_{S,d}}. \tag{C4}$$

Finally we have $\mathrm{Var}[v] \le \frac{1}{\alpha_{S,d}}$. Notice that this inequality can be easily taken equally when $\mathrm{Tr}\left(\rho\gamma_S\right) = 0$.

Appendix D: Details of simplifying $\alpha_{S,d}$ to tensore network

This section shows the details of representing $\alpha_{S,d}$ by the tensor network contraction in PTM representation. According to Lemma 2, the $\alpha_{S,d}$ can be expressed by

$$\alpha_{S,d} = 2^{2n}\langle\langle \mathbf{0},\mathbf{0}|\int \mathrm{d}U_{Q_d}\mathcal{U}_{Q_d}^{\otimes 2}|P_S,P_S\rangle\rangle, \tag{D1}$$

where P_S is the Pauli string corresponding to γ_S via Jordan-Wigner transformation.

Since each two-qubit random matchgate is independently sampled, the integral $\int \mathrm{d}U_Q\mathcal{U}_Q^{\otimes 2}$ can be calculated by independently integrating each 2-qubit matchgate. The result of the integral of the 2-qubit matchgates is given by Lemma 1,

$$\begin{aligned}\int_{U_Q\sim\mathbb{M}_2}\mathrm{d}U_Q\mathcal{U}_Q^{\otimes 2} =& |\gamma_\emptyset\rangle\rangle|\gamma_\emptyset\rangle\rangle\langle\langle\gamma_\emptyset|\langle\langle\gamma_\emptyset| + \frac{1}{4}\sum_{i,j}|\gamma_i\rangle\rangle|\gamma_i\rangle\rangle\langle\langle\gamma_j|\langle\langle\gamma_j| \\ &+ \frac{1}{6}\sum_{\substack{i_1\neq i_2\\ j_1\neq j_2}}|\gamma_{i_1}\gamma_{i_2}\rangle\rangle|\gamma_{i_1}\gamma_{i_2}\rangle\rangle\langle\langle\gamma_{j_1}\gamma_{j_2}|\langle\langle\gamma_{j_1}\gamma_{j_2}| \\ &+ \frac{1}{4}\sum_{\substack{i_1\neq i_2, j_1\neq j_2\\ i_1\neq i_3, j_1\neq j_3\\ i_2\neq i_3, j_2\neq j_3}}|\gamma_{i_1}\gamma_{i_2}\gamma_{i_3}\rangle\rangle|\gamma_{i_1}\gamma_{i_2}\gamma_{i_3}\rangle\rangle\langle\langle\gamma_{j_1}\gamma_{j_2}\gamma_{j_3}|\langle\langle\gamma_{j_1}\gamma_{j_2}\gamma_{j_3}| \\ &+ |\gamma_1\gamma_2\gamma_3\gamma_4\rangle\rangle|\gamma_1\gamma_2\gamma_3\gamma_4\rangle\rangle\langle\langle\gamma_1\gamma_2\gamma_3\gamma_4|\langle\langle\gamma_1\gamma_2\gamma_3\gamma_4|,\end{aligned} \tag{D2}$$

where i, j are index ranged from 1 to 4. Following the definition Eq. (15), each element of tensor $\mathcal{T}$ can be calculated by Eq. (D2). We show these concrete elements in Table I. The tensor $\mathcal{T}$ presents the average effect of a

random two-qubit matchgate.

Here, we represented $|\mathbf{0},\mathbf{0}\rangle\rangle$ in PTM to complete the calculation $\alpha_{S,d} = \langle\langle \mathbf{0},\mathbf{0}|\mathcal{C}|\gamma_S,\gamma_S\rangle\rangle$. Notice the matrix identity

$$|\mathbf{0}\rangle\langle\mathbf{0}| = \frac{1}{2^n}\sum_{\Lambda\subseteq[n]}\prod_{i\in\Lambda} Z_i, \tag{D3}$$

where Z_i denotes the application of the Pauli Z operator to the i-th qubit. Especially, when $\Lambda = \emptyset$, let $\prod_{i\in\Lambda} Z_i = \mathbb{1}_n$. Then, the super vector of $|\mathbf{0},\mathbf{0}\rangle\rangle$ can be expressed as

$$|\mathbf{0},\mathbf{0}\rangle\rangle = \frac{1}{2^{2n}}\sum_{\Lambda,\Lambda'\subseteq[n]} |\prod_{i\in\Lambda} Z_i, \prod_{j\in\Lambda'} Z_j\rangle\rangle. \tag{D4}$$

Eq. (D4) express the supervector $|\mathbf{0},\mathbf{0}\rangle\rangle$ in the PTM representation. Finally, we write the $\mathcal{C}$, $|\mathbf{0},\mathbf{0}\rangle\rangle$, and $|\gamma_S,\gamma_S\rangle\rangle$ in Pauli basis. Thus, the $\alpha_{S,d}$ calculation can be expressed as the tensor network contraction, as illustrated in Fig. 2.

Lemma 2. *The quantity $\alpha_{S,d}$ satisfies the identity $\alpha_{S,d} = 2^{2n}\langle\langle \mathbf{0},\mathbf{0}|\int \mathrm{d}U_{Q_d}\mathcal{U}_{Q_d}^{\otimes 2}|P_S,P_S\rangle\rangle$, where P_S denotes the Pauli string associated with γ_S through the Jordan-Wigner transformation.*

Proof. Follow the definition of $\alpha_{S,d}$, we have

$$\alpha_{S,d} = \int_{Q\sim O_d} \mathrm{d}U_{Q_d}\left|\langle\mathbf{0}|\, U_{Q_d}\gamma_S U_{Q_d}^\dagger\,|\mathbf{0}\rangle\right|^2 \tag{D5}$$

$$= \int_{Q\sim O_d} \mathrm{d}U_{Q_d}\,\langle\mathbf{0}|\, U_{Q_d}\gamma_S U_{Q_d}^\dagger\,|\mathbf{0}\rangle\,\langle\mathbf{0}|\, U_{Q_d}\gamma_S^\dagger U_{Q_d}^\dagger\,|\mathbf{0}\rangle\,. \tag{D6}$$

The subscript d denotes the depth of the matchgate circuit. The expression can be simplified by substituting the relationship between $\gamma_S^\dagger$ and γ_S, which is

$$\gamma_S^\dagger = (-1)^{\frac{|S|(|S|-1)}{2}}\gamma_S, \tag{D7}$$

due to the anti-commutation relation of Majorana operators $\{\gamma_i,\gamma_j\} = 2\delta_{ij}$. The $\alpha_{S,d}$ can be expressed as

$$\alpha_{S,d} = (-1)^{\frac{|S|(|S|-1)}{2}}\int \mathrm{d}U_{Q_d}\,\langle\mathbf{0}|\, U_{Q_d}\gamma_S U_{Q_d}^\dagger\,|\mathbf{0}\rangle^2 \tag{D8}$$

$$= (-1)^{\frac{|S|(|S|-1)}{2}}\int \mathrm{d}U_{Q_d}\,\mathrm{tr}\Big(U_{Q_d}\gamma_S U_{Q_d}^\dagger\,|\mathbf{0}\rangle\,\langle\mathbf{0}|\Big)^2 \tag{D9}$$

$$= (-1)^{\frac{|S|(|S|-1)}{2}}2^{2n}\int \mathrm{d}U_{Q_d}\langle\langle \mathbf{0},\mathbf{0}|\mathcal{U}_{Q_d}^{\otimes 2}|\gamma_S,\gamma_S\rangle\rangle \tag{D10}$$

$$= (-1)^{\frac{|S|(|S|-1)}{2}}2^{2n}\langle\langle \mathbf{0},\mathbf{0}|\int \mathrm{d}U_{Q_d}\mathcal{U}_{Q_d}^{\otimes 2}|\gamma_S,\gamma_S\rangle\rangle. \tag{D11}$$

In PTM representation, the γ_S corresponds to a Pauli basis with a phase $\pm\mathrm{i}^{\lfloor |S|/2\rfloor}$. Thus, the super vector $|\gamma_S,\gamma_S\rangle\rangle$ can be represented as

$$|\gamma_S,\gamma_S\rangle\rangle = (-1)^{\lfloor\frac{|S|}{2}\rfloor}|P_S,P_S\rangle\rangle, \tag{D12}$$

where P_S is the Pauli operator that corresponds to the γ_S.

Follows Eq. (D11) and Eq. (D12), the sign of $\alpha_{S,d}$ is determined by $(-1)^{\frac{|S|(|S|-1)}{2}}(-1)^{\lfloor|S|/2\rfloor}$. We show that the sign equals to 1 by categorizing the parity of $|S|$.

1. **$|S|$ is an odd number.** Let $|S| = 2q+1$, $q\in\mathbb{N}$, $q\geq 0$. And then

$$(-1)^{\frac{|S|(|S|-1)}{2}}(-1)^{\lfloor|S|/2\rfloor} = (-1)^{q(2q+1)+q} = 1. \tag{D13}$$

2. **$|S|$ is an even number.** Let $|S| = 2q$, $q\in\mathbb{N}$, $q\geq 0$. And then

$$(-1)^{\frac{|S|(|S|-1)}{2}}(-1)^{\lfloor|S|/2\rfloor} = (-1)^{(2q-1)q+q} = 1. \tag{D14}$$

Thus, we conclude that the $\alpha_{S,d}$ can be expressed by

$$\alpha_{S,d} = (-1)^{\frac{|S|(|S|-1)}{2}}(-1)^{\lfloor|S|/2\rfloor}2^{2n}\langle\langle \mathbf{0},\mathbf{0}|\int \mathrm{d}U_{Q_d}\mathcal{U}_{Q_d}^{\otimes 2}|P_S,P_S\rangle\rangle \tag{D15}$$

$$= \langle\langle \mathbf{0},\mathbf{0}|\int \mathrm{d}U_{Q_d}\mathcal{U}_{Q_d}^{\otimes 2}|P_S,P_S\rangle\rangle. \tag{D16}$$

□

Appendix E: Mapping the action of tensors to random walk

Here, we give some notations to express the properties of the $\alpha_{S,d}$ tensor network. Let $\mathcal{T}^{(o)}$ represent the odd layer in $\mathcal{C}$, and $\mathcal{T}^{(e)}$ represent the even layer in $\mathcal{C}$, as shown in Fig. 5. Any tensor network $\mathcal{C}$ with brickwork architecture can be expressed by alternately apply $\mathcal{T}^{(o)}$ and $\mathcal{T}^{(e)}$ gates,

$$\mathcal{C}\,(t,b_1,b_2) = \mathcal{T}^{(o)^{b_2}}\mathcal{B}^t\mathcal{T}^{(e)^{b_1}}, \tag{E1}$$

where $b_1,b_2\in\{0,1\}$, $t+b_1+b_2$ stands for the depth, and $\mathcal{B} = \mathcal{T}^{(e)}\mathcal{T}^{(o)}$. Let Γ_n' denote the vectorized double supervector space of Γ_n, defined as $\Gamma_n' = \mathrm{span}\{|\gamma_S,\gamma_S\rangle\rangle \mid \gamma_S\in\Gamma_n\}$. Notably, both $\mathcal{T}^{(o)}$ and $\mathcal{T}^{(e)}$ gates are projection operators, satisfying $(\mathcal{T}^{(e)})^2 = \mathcal{T}^{(e)}$ and $(\mathcal{T}^{(o)})^2 = \mathcal{T}^{(o)}$.

Throughout the main text, we often use the term "representation" without giving a precise definition. In this section, we use language from representation theory to provide a clear and more formal explanation of how $\mathcal{C}$ is represented. As we mentioned in the main text, the whole tensor $\mathcal{C}$ can be expressed by

$$\mathcal{C} = \begin{cases}\mathcal{B}^t, & d = 2t\\ \mathcal{B}^t\mathcal{T}_{\mathrm{init}}, & d = 2t+1.\end{cases} \tag{E2}$$

For the odd-depth case, studying the contraction of $\mathcal{C}$ on Γ_n' is the same as analyzing how the group $\{\mathcal{B}^t\}$ acts on the representation space $\mathcal{T}_{\mathrm{init}}(\Gamma_n')$. A similar approach holds for even depths with $t\geq 1$, except the initial states

TABLE I: Values of tensor $\mathcal{T}$. The head of columns represents the input of $\mathcal{T}$ while the head of rows represents the output of $\mathcal{T}$. For example, the values in row 'XY' and column 'YZ' represent the value $\mathcal{T}^{XY}_{YZ}$. The blank space of the table stands for 0. For example, $\mathcal{T}^{XY}_{YZ}$ is equal to $\frac{1}{6}$.

$\mathcal{T}$	II	IX	IY	IZ	XI	XX	XY	XZ	YI	YX	YY	YZ	ZI	ZX	ZY	ZZ
II	1															
IX		1/4	1/4					1/4				1/4				
IY		1/4	1/4					1/4				1/4				
IZ				1/6		1/6	1/6			1/6	1/6		1/6			
XI					1/4				1/4					1/4	1/4	
XX				1/6		1/6	1/6			1/6	1/6		1/6			
XY				1/6		1/6	1/6			1/6	1/6		1/6			
XZ		1/4	1/4					1/4				1/4				
YI					1/4				1/4					1/4	1/4	
YX				1/6		1/6	1/6			1/6	1/6		1/6			
YY				1/6		1/6	1/6			1/6	1/6		1/6			
YZ		1/4	1/4					1/4				1/4				
ZI				1/6		1/6	1/6			1/6	1/6		1/6			
ZX					1/4				1/4					1/4	1/4	
ZY					1/4				1/4					1/4	1/4	
ZZ																1

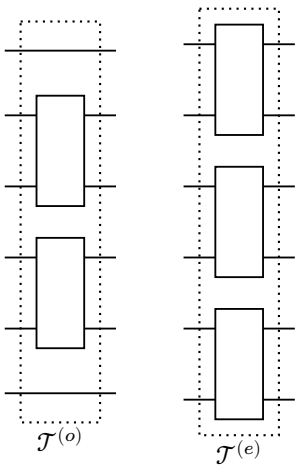

FIG. 5: Illustration for the odd-layer tensor $\mathcal{T}^{(o)}$ and the even-layer tensor $\mathcal{T}^{(e)}$.

differ: for even depth, the initial state is $\mathcal{T}_{\text{init}}|\gamma_S,\gamma_S\rangle\rangle$, while for odd depth, it is $\mathcal{B}|\gamma_S,\gamma_S\rangle\rangle$. Since $\mathcal{B}|\gamma_S,\gamma_S\rangle\rangle$ still lies in $\mathcal{T}_{\text{init}}(\Gamma'_n)$, the same method applies to the even-depth case. Therefore, whether the depth is even or odd, the contraction of $\mathcal{C}$ on Γ'_n can be studied by examining the representation of the group $\{\mathcal{B}^t\}$. We refer to this simply as "the representation of $\mathcal{C}$". To simplify our analysis, we focus on a random circuit with an even number of qubits and an odd depth d. We will represent the contraction of $\mathcal{C}$ in a polynomial space, as shown in Fig. 6.

1. Reduce the calculation to polynomial space

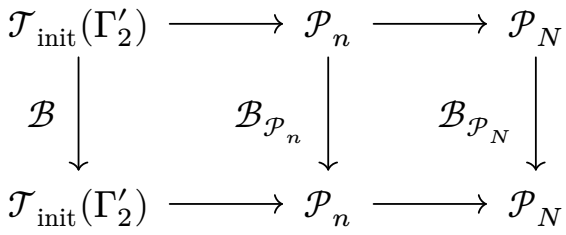

FIG. 6: Illustration for the isometric mapping to the polynomial space. Γ'_2 represents the vectorized double supervector space. Horizontal arrows indicate transitions between spaces, while vertical arrows correspond to the operators $\mathcal{B}$ in different representations. Ultimately, the process is reduced to the N-elementary polynomial within the second-degree polynomial space.

We represent $\mathcal{C}|\gamma_S,\gamma_S\rangle\rangle$ in a polynomial space to allow key operations, such as multiplication and addition, that are essential for our analysis. According to Table I, $\mathcal{T}_{\text{init}}(\Gamma'_2)$ is spanned by operators of the form

$$\begin{cases} |\psi_{ij}\rangle\rangle = & \frac{1}{4}|X_i\left(\prod_{k=i+1}^{j-1} Z_k\right)Y_j\rangle\rangle^{\otimes 2} + \frac{1}{4}|X_i\left(\prod_{k=i+1}^{j-1} Z_k\right)Y_j\rangle\rangle^{\otimes 2} \\ & +\frac{1}{4}|X_i\left(\prod_{k=i+1}^{j-1} Z_k\right)Y_j\rangle\rangle^{\otimes 2} + \frac{1}{4}|X_i\left(\prod_{k=i+1}^{j-1} Z_k\right)Y_j\rangle\rangle^{\otimes 2}, \quad i<j, \\ |\psi_{ii}\rangle\rangle = & |Z_i, Z_i\rangle\rangle. \end{cases} \tag{E3}$$

We define an isometric map $\phi : \mathcal{T}_{\text{init}}(\Gamma_2') \to \mathcal{P}_n$ by setting $\phi(|\psi_{ij}\rangle\rangle) := x_i x_j$ and $\phi(|\psi_{ii}\rangle\rangle) := x_i^2$. This map is a linear isomorphism and a homomorphism with an inverse, which means $\mathcal{T}_{\text{init}}(\Gamma_2')$ and $\mathcal{P}_n$ are isomorphic. We then define the action of $\mathcal{C}$ on $\mathcal{P}_n$ by

$$\mathcal{C}_{\mathcal{P}_n}(\cdot) := \phi \circ \mathcal{C} \circ \phi^{-1}(\cdot). \tag{E4}$$

Consequently, the action of a d-depth matchgate circuit on $\gamma_{\{i,j\}}$ is equivalent to the action of $\mathcal{C}_{\mathcal{P}_n}$ on $x_i x_j$.

By Lemma 3, we can further simplify this representation by identifying a sub-representation $\mathcal{P}_N \subset \mathcal{P}_n$, where $N = \frac{n}{2}$. The variable N is an integer since we have assumed that n is an even number. Certain hidden patterns are revealed by reducing the representation to the polynomial space $\mathcal{P}_N$. Most of the main results are been proved in the $\mathcal{P}_N$.

Lemma 3. *The space $\mathcal{P}_N$ is a faithful representation of $\{\mathcal{B}\}$ restricts on the space $\mathcal{T}_{init}(\Gamma_2')$*

Proof. We begin by defining the group action on $\mathcal{P}_N$ by using $\mathcal{P}_n$ as a medium. Since we have defined the group action on $\mathcal{P}_n$, we want to define the group action on $\mathcal{P}_N$ with the help of $\mathcal{P}_n$. With this idea, we define a linear map φ as

$$\begin{aligned} &\varphi : \mathcal{P}_N \to \mathcal{P}_n \\ &\quad y_i^2 \mapsto x_{2i-1}^2 + 4x_{2i-1}x_{2i} + x_{2i}^2 \\ &\quad y_i y_j \mapsto (x_{2i-1} + x_{2i})(x_{2j-1} + x_{2j}). \end{aligned} \tag{E5}$$

For a general element in $\mathcal{P}_N$, written as $\sum \xi_{ij}\, y_i y_j$, the linearity leads to

$$\varphi\Big(\sum \xi_{ij}\, y_i y_j\Big) := \sum \xi_{ij}\, \varphi(y_i y_j).$$

This makes $\varphi(\mathcal{P}_N)$ a linear subspace of $\mathcal{P}_n$. Because φ is injective, there is a map $\varphi' : \mathcal{P}_n \to \mathcal{P}_N$ such that $\varphi' \circ \varphi$ is the identity on $\mathcal{P}_N$.

The action of $\mathcal{C}$ in $\mathcal{P}_N$ is constructed by

$$\mathcal{C}_{\mathcal{P}_N}(y_i y_j) := \varphi' \circ \mathcal{C}_{\mathcal{P}_n} \circ \varphi(y_i y_j). \tag{E6}$$

Based on the definition of representation, the space $\mathcal{P}_N$ is a representation of $\mathcal{C}$. And Eq. (E6) depicts how to act a tensor on $\mathcal{P}_N$.

The next step is to show that such a representation of $\mathcal{C}$ does not "lose information". Formally, we need to prove that the representation $\mathcal{P}_n$ can be reduced to a sub-representation isometrics to $\mathcal{P}_N$. Naturally, we will consider whether the subspace $\varphi(\mathcal{P}_N)$ will constitute a sub-representation. If it is true, we can reduce the representation to its faithful sub-representation $\varphi(\mathcal{P}_N) \subseteq P_n$, which isometric to the polynomial space $\varphi(\mathcal{P}_N) \simeq \mathcal{P}_N$.

By the definition of sub-representation, we need to prove

$$\mathcal{B}^t(\varphi(\mathcal{P}_N)) \subseteq \varphi(\mathcal{P}_N), \quad \forall t. \tag{E7}$$

The proof of statement (E7) will be carried out using mathematical induction.

When $t = 0$, $\varphi(\mathcal{P}_N) \subseteq \varphi(\mathcal{P}_N)$ is true. Suppose the statement is true for t^*, then we have

$$(\mathcal{T}_{\mathcal{P}_n}^{(e)}\mathcal{T}_{\mathcal{P}_n}^{(o)})^{t^*}(\varphi(y_i y_j)) = \sum \xi_{lm}\varphi(y_l y_m). \tag{E8}$$

And then

$$\begin{aligned} \mathcal{B}_{\mathcal{P}_n}^{t^*+1}(\varphi(y_i y_j)) =& \mathcal{T}_{\mathcal{P}_n}^{(e)}\mathcal{T}_{\mathcal{P}_n}^{(o)}(\sum \xi_{lm}\varphi(y_l y_m)) && \text{(E9)} \\ =& \sum \xi_{lm}\delta_{lm}\mathcal{T}_{\mathcal{P}_n}^{(e)}\mathcal{T}_{\mathcal{P}_n}^{(o)}(x_{2i-1}^2 + 4x_{2i-1}x_{2i} + x_{2i}^2) && \text{(E10)} \\ &+ \sum \xi_{lm}(1-\delta_{lm})\mathcal{T}_{\mathcal{P}_n}^{(e)}\mathcal{T}_{\mathcal{P}_n}^{(o)}\left((x_{2i-1} + x_{2i})(x_{2j-1} + x_{2j})\right), && \text{(E11)} \end{aligned}$$

where $\mathcal{B}_{\mathcal{P}_n}$, $\mathcal{T}_{\mathcal{P}_n}^{(e)}$ and $\mathcal{T}_{\mathcal{P}_n}^{(o)}$ are defined in a manner analogous to $\mathcal{C}_{\mathcal{P}_n}$. We will prove Eq. (E10) is in the space $\varphi(\mathcal{P}_N)$,

while the same result of Eq. (E11) can be proved by straightforward calculation

$$\begin{aligned}
&\mathcal{T}^{(e)}_{\mathcal{P}_n}\mathcal{T}^{(o)}_{\mathcal{P}_n}(x^2_{2i-1}+4x_{2i-1}x_{2i}+x^2_{2i})\\
=&\mathcal{T}^{(e)}_{\mathcal{P}_n}(\frac{1}{6}x^2_{2i-2}+\frac{2}{3}x_{2i-2}x_{2i-1}+x_{2i-2}x_{2i}+x_{2i-2}x_{2i+1}\\
&+\frac{1}{6}x^2_{2i-1}+x_{2i-1}x_{2i}+x_{2i-1}x_{2i+1}+\frac{1}{6}x^2_{2i}+\frac{2}{3}x_{2i}x_{2i+1}+\frac{1}{6}x^2_{2i+1})\\
=&\frac{1}{36}x^2_{2i-3}+\frac{1}{9}x_{2i-3}x_{2i-2}+\frac{5}{12}x_{2i-3}x_{2i-1}+\frac{5}{12}x_{2i-3}x_{2i}+\frac{1}{4}x_{2i-3}x_{2i+1}+\frac{1}{4}x_{2i-3}x_{2i+2}\\
&+\frac{1}{36}x^2_{2i-2}+\frac{5}{12}x_{2i-2}x_{2i-1}+\frac{5}{12}x_{2i-2}x_{2i}+\frac{1}{4}x_{2i-2}x_{2i+1}+\frac{1}{4}x_{2i-2}x_{2i+2}\\
&+\frac{2}{9}x^2_{2i-1}+\frac{8}{9}x_{2i-1}x_{2i}+\frac{5}{12}x_{2i-1}x_{2i+1}+\frac{5}{12}x_{2i-1}x_{2i+2}\\
&+\frac{2}{9}x^2_{2i}+\frac{5}{12}x_{2i}x_{2i+1}+\frac{5}{12}x_{2i}x_{2i+2}+\frac{1}{36}x^2_{2i+1}+\frac{1}{9}x_{2i+1}x_{2i+2}+\frac{1}{36}x^2_{2i+2}
\end{aligned} \tag{E12}$$

The result expression is in $\varphi(\mathcal{P}_N)$ because we can find a polynomial y in $\mathcal{P}_N$ such that $\varphi(y)$ equals the result expression,

$$\begin{aligned}
y=&\frac{1}{6}y^2_{i-1}+\frac{5}{3}y_{i-1}y_i+y_{i-1}y_{i+1}+\frac{4}{3}y^2_i\\
&+\frac{5}{3}y_{i-1}y_{i+1}+\frac{1}{6}y^2_{i+1}
\end{aligned} \tag{E13}$$

$$\varphi(y)=\mathcal{T}^{(e)}_{\mathcal{P}_n}\mathcal{T}^{(o)}_{\mathcal{P}_n}(x^2_{2i-1}+4x_{2i-1}x_{2i}+x^2_{2i}) \tag{E14}$$

Thus, we get that

$$\mathcal{B}_{\mathcal{P}_n}(x^2_{2i-1}+4x_{2i-1}x_{2i}+x^2_{2i})\subseteq\varphi(\mathcal{P}_N), \tag{E15}$$

which complete the proof of statement E7.

We aim to show that $\varphi(\mathcal{P}_N)$ is a faithful sub-representation. Suppose, for the sake of contradiction, that $\varphi(\mathcal{P}_N)$ is not faithful. Then, there exists a non-zero element $y\in\mathcal{P}_N$ such that:

$$\varphi(y)\neq 0 \quad\text{and}\quad \mathcal{B}^t_{\mathcal{P}_n}(\varphi(y))=0 \quad\text{for some integer } t\geq 1.$$

Consider applying the operator $\mathcal{B}^{t'}_{\mathcal{P}_n}$ iteratively to both sides of the equation:

$$\mathcal{B}^{t'}_{\mathcal{P}_n}\left[\mathcal{B}^t_{\mathcal{P}_n}(\varphi(y))\right]=\mathcal{B}^{t+t'}_{\mathcal{P}_n}(\varphi(y))=\mathcal{B}^{t'}_{\mathcal{P}_n}(0)=0.$$

Taking the limit as $t'\to\infty$, we obtain:

$$\lim_{t'\to\infty}\mathcal{B}^{t+t'}_{\mathcal{P}_n}(\varphi(y))=0.$$

However, the infinite application of $\mathcal{B}_{\mathcal{P}_n}$ to $\varphi(y)$ yields a non-zero polynomial. This is a contradiction because the same expression cannot simultaneously be zero and non-zero. Therefore, our initial assumption that $\varphi(\mathcal{P}_N)$ is not faithful must be false. Hence, $\varphi(\mathcal{P}_N)$ is indeed a faithful sub-representation.

□

2. Mapping the spread of polynomials to random walk

We can calculate the output of $\mathcal{B}_{\mathcal{P}_N}(y_iy_j)$ by $\mathcal{B}_{\mathcal{P}_N}(y_iy_j):=\varphi'\circ\phi^{-1}\circ\mathcal{B}\circ\phi\circ\varphi(y_iy_j)$, and the results are shown in Table II. The definition of function L is

$$L(y_i)=\begin{cases}\frac{3}{4}y_1+\frac{1}{4}y_2, & i=1\\ \frac{1}{4}y_{i-1}+\frac{1}{2}y_i+\frac{1}{4}y_{i+1}, & 1<i<N\\ \frac{3}{4}y_N+\frac{1}{4}y_{N-1}, & i=N.\end{cases} \tag{E16}$$

Notice that for most cases, the subscripts i,j satisfy $1<i<N-1$ and $i+1<j\leq N$, then the outcomes of $\mathcal{B}_{\mathcal{P}_N}$ is

$$\begin{aligned}
\mathcal{B}_{\mathcal{P}_N}(y_iy_j)=&\left(\frac{1}{4}y_{i-1}+\frac{1}{2}y_i+\frac{1}{4}y_{i-1}\right)\\
&\times\left(\frac{1}{4}y_{j-1}+\frac{1}{2}y_j+\frac{1}{4}y_{j-1}\right).
\end{aligned} \tag{E17}$$

In this case, the action of $\mathcal{B}_{\mathcal{P}_N}$ can be viewed as independently evolving y_i and y_j in a one-dimensional lattice (see Fig. 7)

$$\begin{aligned}
y_i&\to\frac{1}{4}y_{i-1}+\frac{1}{2}y_i+\frac{1}{4}y_{i-1}\\
y_j&\to\frac{1}{4}y_{j-1}+\frac{1}{2}y_j+\frac{1}{4}y_{j-1}.
\end{aligned} \tag{E18}$$

Here, we interpreted $y_1,\cdots y_n$ as a finite one-dimensional lattice whose i-th site is labeled by y_i. The action of $\mathcal{B}_{\mathcal{P}_N}$ can be interpreted as a random walk on 2D lattice whose (i,j) site is labeled by y_iy_j. We observe that the equation $\mathcal{B}_{\mathcal{P}_N}(y_iy_j)=L(y_i)L(y_j)$ holds for most sites. This observation inspires us to first analyze the evolving behavior of L and then use the probability distribution of L to estimate the order of $\alpha_{S,d}$.

We introduce the symmetry lazy random walk (SLRW) in polynomial space, or the one-dimensional lattice, to describe the evolution behavior of L. A SLRW is a type of

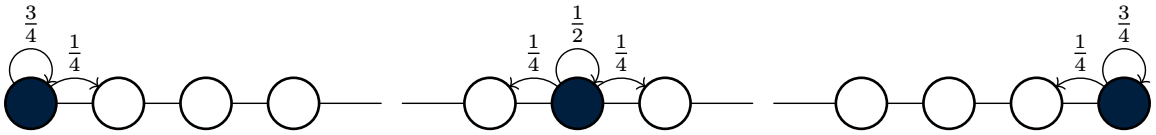

FIG. 7: Illustration of lazy symmetry random walk.

Markov process shown in Fig. 7. In this process, consider a point located at a site y_i. In the next time interval, this point has a probability of 0.25 moving to one of its neighboring sites y_{i-1} or y_{i+1}, and it has a probability of 0.5 staying in place. If the origin site is on the ends of the lattice, it has a probability of 0.75 staying in place and has a probability of 0.25 moving around. The probability transition relation can be expressed by Eq. (E16). We can see that the separate evolution in Eq. (E18) fits the form of SLRW. The transition step $\mathcal{L}_{\Gamma_2}$ in the representation space Γ_2' can be given by

$$\mathcal{L}_{\Gamma_2}|\gamma_S,\gamma_S\rangle\rangle = (L\times L)\circ\varphi'\circ\phi(|\gamma_S,\gamma_S\rangle\rangle), \tag{E19}$$

where $(L\times L)(y_iy_j) = L(y_i)L(y_j)$.

In Eq. (E17), we showed the result of how y_iy_j transfers in one specific situation. Now, we will show all possible results in any situation in Table II. The table lists all the possible transition results no matter what inputs it receives. It was created in a similar way to the previous example in Eq. (E12).

In Table II, we can see that in most cases

$$\mathcal{B}_{\mathcal{P}_N}(y_iy_j) = L(y_i)L(y_j) \tag{E20}$$

except for the cases when $|i-j|\le 1$. When $|i-j|\le 1$, the coefficients of remainder terms $\mathcal{B}_{\mathcal{P}_N}(y_iy_j) - L(y_i)L(y_j)$ are small. Denote $L^t(y_i)$ as the outcome of SLRW t-steps from y_i according to the propagation rule in Eq. (E16), and the $\mathcal{L}_i(\mu,t)$ as the probability of stopping at y_μ after t-steps walking,

$$L^t(y_i) = \sum_\mu \mathcal{L}_i(\mu,t)y_\mu. \tag{E21}$$

Refs. [37] gives the analytical solution of $\mathcal{L}_i$, which is

$$\begin{aligned}\mathcal{L}_i(\mu,t) = \frac{1}{N} + \frac{2}{N}\sum_{k=1}^{N-1}\cos\left(\left(\mu-\frac{1}{2}\right)\frac{\pi k}{N}\right)\\ \times\cos\left(\left(i-\frac{1}{2}\right)\frac{\pi k}{N}\right)\cos^{2t}\left(\frac{\pi k}{2N}\right).\end{aligned} \tag{E22}$$

Thus, for the evolution that can be separated by $\mathcal{B}_{\mathcal{P}_N}(y_iy_j) = L(y_i)L(y_j)$, we can get the analytical solution results

$$\mathcal{C}_{\mathcal{P}_N}(y_iy_j) = (\mathcal{B}_{\mathcal{P}_N})^t(y_iy_j) \tag{E23}$$

$$= L^t(y_i)L^t(y_j) + R(y_iy_j) \tag{E24}$$

$$= \sum_{\mu,\nu}\left(\mathscr{L}_{ij}(\mu,\nu,t)y_\mu y_\nu + \mathscr{R}_{ij}(\mu,\nu,t)y_\mu y_\nu\right), \tag{E25}$$

where

$$\mathscr{L}_{ij}(\mu,\nu,t) := \mathcal{L}_i(\mu,t)\mathcal{L}_j(\nu,t), \tag{E26}$$

and R stands for the reminder terms caused by the near-diagonal terms y_iy_j, $|i-j|\le 1$ in Table II.

The computation of $\alpha_{S,d}$ can be divided into two primary components: one originating from the SLRW and the other arising from the remainder terms. Specifically, $\alpha_{S,d}$ is determined through the tensor contraction of the operator $\mathcal{C}$, the state $|P_S\rangle\rangle$, and the state $|\mathbf{0},\mathbf{0}\rangle\rangle$. To facilitate this calculation, both $\mathcal{C}$ and $|P_S\rangle\rangle$ have been mapped into polynomial space. Similarly, the state $|\mathbf{0},\mathbf{0}\rangle\rangle$ is also represented within this polynomial framework.

Eq. (D4) plays a crucial role in this process by transforming $|\mathbf{0},\mathbf{0}\rangle\rangle$ into the Pauli basis. In this context, $\langle\langle Z_i|$ acts as a projection operator that converts a supervector into a scalar. Specifically, $\langle\langle Z_i|$ maps the supervector $|Z_i\rangle\rangle$ to 1 while mapping all other Pauli basis vectors to 0. As previously established, the supervector $|Z_i\rangle\rangle$ is associated with the monomial x_i^2 in the polynomial space $\mathcal{P}_n$.

Recognizing that the space of derivative operators constitutes the dual space to $\mathcal{P}_n$, we employ these operators to represent the dual space of $\mathcal{P}_n$. In this representation, the dual vectors are mapped as

$$\langle\langle\psi_{ij}| \to \frac{\partial^2}{\partial x_i\partial x_j},\quad \langle\langle\psi_{ii}| \to \frac{1}{2}\frac{\partial^2}{\partial x_i^2}. \tag{E27}$$

This mapping ensures that the action of the dual vectors on the polynomial space corresponds to differentiation operations, which are fundamental in analyzing the system's behavior.

Using analogous methods and performing the necessary algebraic manipulations, we extend this mapping to transform $\langle\langle\mathbf{0},\mathbf{0}|$ into the polynomial space $\mathcal{P}_N$ for the case where $|S| = 2$. gives the resulting expression

$$\langle\langle\mathbf{0},\mathbf{0}| \to \frac{1}{6}\sum_i\frac{\partial^2}{\partial y_i^2}. \tag{E28}$$

y_iy_j	$\mathcal{B}_{\mathcal{P}_N}(y_iy_j)$
$i=j=1$	$L(y_i)L(y_j)-\frac{5}{144}y_1y_1-\frac{5}{144}y_2y_2+\frac{5}{72}y_1y_2$
$1<i<N, j=i$	$L(y_i)L(y_j)-\frac{5}{144}y_{i-1}y_{i-1}+\frac{1}{36}y_{i-1}y_i+\frac{1}{24}y_{i-1}y_{i+1}-\frac{1}{36}y_iy_i+\frac{1}{36}y_iy_{i+1}-\frac{5}{144}y_{i+1}y_{i+1}$
$1\le i<N, j=i+1$	$L(y_i)L(y_j)-\frac{1}{48}y_iy_i-\frac{1}{48}y_{i+1}y_{i+1}+\frac{1}{24}y_iy_{i+1}$
$i=j=N$	$L(y_i)L(y_j)-\frac{5}{144}y_Ny_N-\frac{5}{144}y_{N-1}y_{N-1}+\frac{5}{72}y_{N-1}y_N$
otherwise	$L(y_i)L(y_j)$

TABLE II: The transition result of $\mathcal{B}_{\mathcal{P}_N}$ with input y_iy_j in different condition. Notice that $y_iy_j = y_jy_i$, the indices of the two factors i and j in term y_iy_j can always be arranged in ascending order $i\le j$.

This transformation incorporates factor $\frac{1}{6}$, which arises from the definitions of the Pauli and polynomial bases. Subsequently, the $\alpha_{S,2t+1}$ for odd depth $d=2t+1$ can be expressed in terms of these derivative operators and the action of $\mathcal{C}$ within the polynomial space $\mathcal{P}_N$

$$\alpha_{\{\gamma_i\gamma_j\},2t+1}=\frac{1}{6}\sum_{\mu}\frac{\partial^2}{\partial y_\mu^2}\mathcal{C}_{\mathcal{P}_N}(y_iy_j). \tag{E29}$$

By combining Equation (E25) with Equation (E29), we obtain:

$$\alpha_{\{\gamma_i\gamma_j\},2t+1}=\frac{1}{3}\sum_{\mu}\mathscr{L}_{ij}(\mu,\mu,t)+\frac{1}{3}\sum_{\mu}\mathscr{R}_{ij}(\mu,\mu,t) \tag{E30}$$

$$=:\alpha^L_{\{\gamma_i\gamma_j\},2t+1}+\alpha^R_{\{\gamma_i\gamma_j\},2t+1}, \tag{E31}$$

where $\mathscr{L}_{ij}(\mu,\mu,t)$ represents a transition probability associated with the SLRW, and $\mathscr{R}_{ij}(\mu,\mu,t)$ corresponds to the reminders.

Appendix F: Estimate the order of $\alpha^L_{\{\gamma_i\gamma_j\},2t+1}$

We have separated the calculation of $\alpha_{\{\gamma_i\gamma_j\},2t+1}$ into two parts in Sec. E 2. In this section, we aim to estimate the order of the first part, $\alpha^L_{\{\gamma_i\gamma_j\},2t+1}$.

Lemma 4. *The following formula can estimate the* $\alpha^L_{\{\gamma_i\gamma_j\},2t+1}$

$$\alpha^L_{\{\gamma_i\gamma_j\},2t+1}=\frac{1}{3\sqrt{2\pi t}}\sum_{k=-\infty}^{\infty}\left(e^{-\frac{(2Nk+a)^2}{2t}}+e^{-\frac{(2Nk+b)^2}{2t}}\right)+\mathcal{O}\left(e^{-\frac{\pi^2}{2}t}\right) \tag{F1}$$

where a is defined as $|i-j|$ and b is defined as $i+j-1$.

Proof. Recall that $N=n/2$. By Lemma 6, the expression for $\alpha_{S,2t+1}$ can be simplified to the form given in Eq. (F15). Moreover, adding the term corresponding to $k=0$ does not affect the summation series,

$$3\alpha^L_{\{\gamma_i\gamma_j\},2t+1}=-\frac{1}{N}+\frac{1}{N}\sum_{k=0}^{N-1}\left[\cos\left((i-j)\frac{k\pi}{N}\right)+\cos\left((i+j-1)\frac{k\pi}{N}\right)\right]\cos^{4t}\left(\frac{\pi k}{2N}\right). \tag{F2}$$

Hence, the summation over k spans a complete cycle, enabling us to leverage certain useful properties of trigonometric summations.

Our goal is to use the Poisson summation formula to estimate the order of $\alpha_{S,d}$. To facilitate this, it is more practical to express the formula using exponentials rather than trigonometric functions. Note that e^{-2tx^2} serves as a good approximation for $\cos^{4t}(x)$,

$$\begin{aligned}e^{-2tx^2}-\cos^{4t}(x)&=e^{-2tx^2}-e^{-2tx^2+O\left(tx^4\right)}\\&=e^{-2tx^2}\left(1-e^{O\left(tx^4\right)}\right)\\&\sim\mathcal{O}\left(tx^4e^{-2tx^2}\right).\end{aligned} \tag{F3}$$

By substituting $\cos^{4t}\left(\frac{\pi k}{2N}\right)$ with $e^{-\frac{k^2\pi^2t}{2N^2}}$ in Eq. (F2), we have

$$3\alpha^L_{\{\gamma_i\gamma_j\},2t+1} = -\frac{1}{N} + \frac{1}{N}\sum_{k=0}^{N-1} e^{-\frac{k^2\pi^2 t}{2N^2}}\left[\cos\left((i-j)\frac{k\pi}{N}\right) + \cos\left((i+j-1)\frac{k\pi}{N}\right)\right] + \mathcal{O}\left(e^{-\frac{\pi^2}{2}t}\right) \tag{F4}$$

$$= -\frac{1}{N} + \frac{1}{N}\sum_{k=0}^{\infty} e^{-\frac{k^2\pi^2 t}{2N^2}}\left[\cos\left((i-j)\frac{k\pi}{N}\right) + \cos\left((i+j-1)\frac{k\pi}{N}\right)\right] + \mathcal{O}\left(e^{-\frac{\pi^2}{2}t}\right). \tag{F5}$$

In Eq. (F5), we expand the summation to infinity, and it will not introduce much of errors because

$$\begin{aligned}\sum_{k=N}^{\infty} e^{-\frac{k^2\pi^2 t}{2N^2}} =& e^{-\frac{\pi^2}{2}t}\sum_{k=0}^{\infty} e^{-\frac{k^2\pi^2 t}{2N^2}}\\ \leq& e^{-\frac{\pi^2}{2}t}\sum_{k=0}^{\infty} e^{-\frac{k\pi^2 t}{2N^2}}\\ =& e^{-\frac{\pi^2}{2}t}\frac{e^{\frac{\pi^2 t}{2N^2}}}{e^{\frac{\pi^2 t}{2N^2}}-1}\\ =& \mathcal{O}\left(e^{-\frac{\pi^2}{2}t}\right)\end{aligned}$$

According to the Poison summation formula,

$$\begin{aligned}&\sum_{k=-\infty}^{\infty} e^{-\frac{k^2\pi^2 t}{2N^2}}\cos\left((i-j)\frac{k\pi}{N}\right)\\ =&N\sqrt{\frac{2}{\pi t}}\sum_{k=-\infty}^{\infty} e^{-\frac{(2Nk+i-j)^2}{2t}}\end{aligned} \tag{F6}$$

By substituting Eq. (F6) into Eq. (F5), we have

$$\alpha^L_{\{\gamma_i\gamma_j\},2t+1} \tag{F7}$$

$$= \frac{1}{3\sqrt{2\pi t}}\sum_{k=-\infty}^{\infty}\left(e^{-\frac{(2Nk+i-j)^2}{2t}} + e^{-\frac{(2Nk+i+j-1)^2}{2t}}\right) \tag{F8}$$

$$+ \mathcal{O}\left(e^{-\frac{\pi^2}{2}t}\right). \tag{F9}$$

□

In the following, we give the relationship between $\alpha^L_{S,d}$ with the depth of random matchgate circuits.

Lemma 5. *The $\alpha^L_{S,d}$ scales $\mathcal{O}\left(\frac{1}{\text{poly}(n)}\right)$ if $d = \Theta\left(\max\left\{\frac{d_{int}(S)^2}{\log(n)}, d_{int}(S)\right\}\right)$.*

Proof. We start by proving that

$$\sum_{k=q+1}^{\infty} e^{-\frac{(2Nk+i-j)^2}{2t}} = \mathcal{O}\left(e^{-\frac{(2Nq+i-j)^2}{2t}}\right) \tag{F10}$$

for positive integer q:

$$\frac{\sum_{k=q+1}^{\infty} e^{-\frac{(2Nk+i-j)^2}{2t}}}{e^{-\frac{(2Nq+i-j)^2}{2t}}} \tag{F11}$$

$$= \sum_{k=q+1}^{\infty}\exp\left[\frac{(2Nq+i-j)^2}{2t} - \frac{(2Nk+i-j)^2}{2t}\right] \tag{F12}$$

$$= \sum_{k=q+1}^{\infty}\exp\left[-\frac{2N(k-q)(N(q+k)-(i-j))}{t}\right] \tag{F13}$$

$$\leq \sum_{k=q+1}^{\infty}\exp\left[-\frac{2N(k-q)(2Nq-(i-j))}{t}\right], \tag{F14}$$

where $\sum_{k=q+1}^{\infty}\exp\left[-\frac{2N(k-q)(2Nq-(i-j))}{t}\right]$ converges to certain constant. Thus, we prove Eq. (F10).

Eq. (F10) indicates that the order of $\alpha^L_{S,d}$ is determined by $\frac{1}{\sqrt{2\pi t}}e^{-\frac{(i-j)^2}{2t}} + \mathcal{O}\left(e^{-\frac{\pi^2}{2}t}\right)$. The condition $d = 2t+1 = \Omega(d_{\text{int}})$ ensures that $\mathcal{O}\left(e^{-\frac{\pi^2}{2}t}\right) = \mathcal{O}\left(\frac{1}{\text{poly}(n)}\right)$, while the condition $d = \Omega(\frac{d_{\text{int}}(S)^2}{\log(n)})$ ensures that $e^{-\frac{(i-j)^2}{2t}} = \Omega\left(\frac{1}{\text{poly}(n)}\right)$ (notice that $d_{\text{int}}(S) = |i-j|$ for 2-local Majorana γ_S). Thus, we conclude that $\alpha^L_{S,d} = \Omega\left(\frac{1}{\text{poly}(n)}\right)$ when $d = \Theta\left(\max\left\{\frac{d_{\text{int}}(S)^2}{\log(n)}, d_{\text{int}}(S)\right\}\right)$.

□

Lemma 6. *The expression of $\alpha^L_{\{\gamma_i\gamma_j\},2t+1}$ can be simplified in the following form*

$$\begin{aligned}3\alpha^L_{\{\gamma_i\gamma_j\},2t+1} = \frac{1}{N} + \frac{1}{N}\sum_k\Big[&\cos\left((i-j)\frac{k\pi}{N}\right)\\ &+\cos\left((i+j-1)\frac{k\pi}{N}\right)\Big]\cos^{4t}\left(\frac{\pi k}{2N}\right).\end{aligned} \tag{F15}$$

Proof. By the definition of $\alpha^L_{\{\gamma_i\gamma_j\},2t+1}$ and Eq. E26, we have

$$
\begin{aligned}
3\alpha^{L}_{\{\gamma_i\gamma_j\},2t+1} =& \sum_{\mu}\left[\frac{1}{N}+\frac{2}{N}\sum_{k=1}^{N-1}\cos\left(\left(i-\frac{1}{2}\right)\frac{\pi k}{N}\right)\cos\left(\left(\mu-\frac{1}{2}\right)\frac{\pi k}{N}\right)\cos^{2t}\left(\frac{\pi k}{2N}\right)\right] \\
&\times\left[\frac{1}{N}+\frac{2}{N}\sum_{l=1}^{N-1}\cos\left(\left(j-\frac{1}{2}\right)\frac{\pi l}{N}\right)\cos\left(\left(\mu-\frac{1}{2}\right)\frac{\pi l}{N}\right)\cos^{2t}\left(\frac{\pi l}{2N}\right)\right] \\
=& 1/N+\frac{2}{N^2}\sum_{k}\left[\sum_{\mu}\cos\left(\left(\mu-\frac{1}{2}\right)\frac{\pi k}{N}\right)\right]\cos\left(\left(i-\frac{1}{2}\right)\frac{\pi k}{N}\right)\cos^{2t}\left(\frac{\pi k}{2N}\right) \qquad \text{(F16)} \\
&+\frac{2}{N^2}\sum_{l}\left[\sum_{\mu}\cos\left(\left(\mu-\frac{1}{2}\right)\frac{\pi l}{N}\right)\right]\cos\left(\left(i-\frac{1}{2}\right)\frac{\pi l}{N}\right)\cos^{2t}\left(\frac{\pi l}{2N}\right) \qquad \text{(F17)} \\
&+\frac{4}{N^2}\sum_{k,l=1}^{N-1}\sum_{\mu=1}^{N}\cos\left(\left(i-\frac{1}{2}\right)\frac{\pi k}{N}\right)\cos\left(\left(\mu-\frac{1}{2}\right)\frac{\pi k}{N}\right)\cos^{2t}\left(\frac{\pi k}{2N}\right) \\
&\times\cos\left(\left(j-\frac{1}{2}\right)\frac{\pi l}{N}\right)\cos\left(\left(\mu-\frac{1}{2}\right)\frac{\pi l}{N}\right)\cos^{2t}\left(\frac{\pi l}{2N}\right) \qquad \text{(F18)}
\end{aligned}
$$

Notice that the summation of cosine function is zero

$$
\begin{aligned}
\sum_{\mu=1}^{N}\cos\left(\left(\mu-\frac{1}{2}\right)\frac{\pi k}{N}\right) &= -\frac{1}{2}\cos\left(\frac{1}{2}\pi(2k+1)\right)\csc\left(\frac{\pi k}{2N}\right) \\
&= \sin(k\pi)\csc\left(\frac{\pi k}{2N}\right) \\
&= 0.
\end{aligned} \qquad \text{(F19)}
$$

Substitute this identity into Eq. (F18), we can eliminate the terms in Eqs. (F16) and (F17).

Also, notice that

$$
\begin{aligned}
&\sum_{\mu=1}^{N}\cos\left(\frac{\pi\left(\mu-\frac{1}{2}\right)i}{N}\right)\cos\left(\frac{\pi\left(\mu-\frac{1}{2}\right)j}{N}\right) \\
=&\frac{1}{2}\sum_{\mu=1}^{N}\cos\left(\frac{\pi\left(\mu-\frac{1}{2}\right)i}{N}-\frac{\pi\left(\mu-\frac{1}{2}\right)j}{N}\right)+\cos\left(\frac{\pi\left(\mu-\frac{1}{2}\right)i}{N}+\frac{\pi\left(\mu-\frac{1}{2}\right)j}{N}\right) \\
=&\frac{1}{2}\sum_{\mu=1}^{N}\cos\left(\frac{\pi(2\mu-1)(i-j)}{2N}\right)+\cos\left(\frac{\pi(2\mu-1)(i+j)}{2N}\right) \\
=&\frac{1}{4}\left(\sin(\pi(i+j))\csc\left(\frac{\pi(i+j)}{2N}\right)-\sin(\pi(j-i))\csc\left(\frac{\pi(i-j)}{2N}\right)\right).
\end{aligned} \qquad \text{(F20)}
$$

This result gets value 0 when $\frac{\pi(i+j)}{2N}\neq a\pi$ or $\frac{\pi(i-j)}{2N}\neq b\pi$ for some integer a and b, because $\sin(\pi m)=0$. The term $\sin(\pi m)\csc\left(\frac{\pi m}{2N}\right)$ gets non-zero only when $\csc\left(\frac{\pi m}{2N}\right)$ gets infinity. Then, we can write down the conditions that i and j satisfy

$$
\begin{cases}
i+j=2aN \text{ or } |i-j|=2bN \\
a,b\in\mathbb{Z} \\
1<i,j<N-1.
\end{cases} \qquad \text{(F21)}
$$

The equation shows that the result is $j=k$. We can use L'Hôpital's rule to calculate the term

$$
\lim_{x\to 0}\sin(\pi x)\csc\left(\frac{\pi x}{2N}\right)=2N \qquad \text{(F22)}
$$

when i and j satisfy the condition $i=j$. Plugin Eq. (F22) and Eq. (F20) into Eq. (F18), we have

$$
\begin{aligned}
3\alpha^{L}_{\{\gamma_i\gamma_j\},2t+1} =& \frac{1}{N}+\frac{2}{N}\sum_{k}\cos\left(\left(i-\frac{1}{2}\right)\frac{\pi k}{N}\right) \\
&\times\cos\left(\left(j-\frac{1}{2}\right)\frac{\pi k}{N}\right)\cos^{4t}\left(\frac{\pi k}{2N}\right).
\end{aligned} \qquad \text{(F23)}
$$

Finally, we use trigonometric identities to expand this equation, thereby completing this proof

$$3\alpha^L_{\{\gamma_i\gamma_j\},2t+1} = \frac{1}{N} + \frac{1}{N}\sum_k \Big[\cos\left((i-j)\frac{k\pi}{N}\right) + \cos\left((i+j-1)\frac{k\pi}{N}\right)\Big]\cos^{4t}\left(\frac{\pi k}{2N}\right). \tag{F24}$$

□

Appendix G: The relation between $\alpha^L_{\{\gamma_i\gamma_j\},2t+1}$ and $\alpha^R_{\{\gamma_i\gamma_j\},2t+1}$

Recall that we have divided the calculation of $\alpha_{\{\gamma_i\gamma_j\},2t+1}$ into two parts. One is the $\alpha^L_{\{\gamma_i\gamma_j\},2t+1}$ and the other is $\alpha^R_{\{\gamma_i\gamma_j\},2t+1}$. Lemma 4 gives the order of $\alpha^L_{\{\gamma_i\gamma_j\},2t+1}$. In this section, we aim to bound the $\alpha^R_{\{\gamma_i\gamma_j\},2t+1}$ by $\alpha^L_{\{\gamma_i\gamma_j\},2t+1}$, so that the order of $\alpha_{\{\gamma_i\gamma_j\},2t+1}$ can be given by the $\alpha^L_{\{\gamma_i\gamma_j\},2t+1}$.

We begin with the polynomial in Eq. (E25)

$$\mathcal{C}_{\mathcal{P}_N}(t)(y_iy_j) = \sum_{\mu,\nu}\left(\mathscr{L}_{ij}(\mu,\nu,t)y_\mu y_\nu + \mathscr{R}_{ij}(\mu,\nu,t)y_\mu y_\nu\right). \tag{G1}$$

Notice that the $\mathscr{R}_{ij}$ is the corresponding term of Δ (see the main text, Eq. (22)) in the polynomial space $\mathcal{P}_N$ Then, we let the polynomial transform one time-interval step, and we get

$$\begin{aligned}
&\mathcal{C}_{\mathcal{P}_N}(t+1)(y_iy_j) && \text{(G2)}\\
=&\mathcal{B}_{\mathcal{P}_N}\left(\mathcal{C}_{\mathcal{P}_N}(t)(y_iy_j)\right) && \text{(G3)}\\
=&\sum_{\mu,\nu}\left(\mathscr{L}_{ij}(\mu,\nu,t)(L(y_\mu)L(y_\nu)+R(y_\mu,y_\nu)) + \mathscr{R}_{ij}(\mu,\nu,t)(L(y_\mu)L(y_\nu)+R(y_\mu,y_\nu))\right) && \text{(G4)}\\
=&\sum_{\mu,\nu}\left(\mathscr{L}_{ij}(\mu,\nu,t)(L(y_\mu)L(y_\nu)+R(y_\mu,y_\nu)) + \mathscr{R}_{ij}(\mu,\nu,t)(L(y_\mu)L(y_\nu)+R(y_\mu,y_\nu))\right) && \text{(G5)}\\
=&\sum_{\mu,\nu}\mathscr{L}_{ij}(\mu,\nu,t+1)y_\mu y_\nu + \sum_{\mu,\nu}\mathscr{L}_{ij}(\mu,\nu,t)R(y_\mu,y_\nu)\\
&+\sum_{\mu,\nu}\mathscr{R}_{ij}(\mu,\nu,t)(L(y_\mu)L(y_\nu)+R(y_\mu,y_\nu)). && \text{(G6)}
\end{aligned}$$

Deduce from Eq. (G1), we have

$$\mathcal{C}_{\mathcal{P}_N}(t+1)(y_iy_j) = \sum_{\mu,\nu}\left(\mathscr{L}_{ij}(\mu,\nu,t+1)y_\mu y_\nu + \mathscr{R}_{ij}(\mu,\nu,t+1)y_\mu y_\nu\right). \tag{G7}$$

Compare Eq. (G6) and Eq. (G7), we have

$$\sum_{\mu,\nu}\mathscr{R}_{ij}(\mu,\nu,t+1)y_\mu y_\nu = \sum_{\mu,\nu}\mathscr{L}_{ij}(\mu,\nu,t)R(y_\mu,y_\nu) + \sum_{\mu,\nu}\mathscr{R}_{ij}(\mu,\nu,t)(L(y_\mu)L(y_\nu)+R(y_\mu,y_\nu)) \tag{G8}$$

$$(1+\delta_{l,k})\mathscr{R}_{ij}(l,k,t+1) = \sum_{\mu,\nu}\mathscr{R}_{ij}(\mu,\nu,t)\frac{\partial^2 L(y_\mu)L(y_\nu)}{\partial y_l\partial y_k} + \sum_{\mu,\nu}\left(\mathscr{L}_{ij}(\mu,\nu,t)+\mathscr{R}_{ij}(\mu,\nu,t)\right)\frac{\partial^2 R(y_\mu,y_\nu)}{\partial y_l\partial y_k}. \tag{G9}$$

Eq. (G9) describes the strict relationship between $\mathscr{R}_{ij}$ and $\mathscr{L}_{ij}$ in a recursive form, thereby giving the relationship between $\alpha^L_{\{\gamma_i\gamma_j\},2t+1}$ and $\alpha^R_{\{\gamma_i\gamma_j\},2t+1}$. However, deriving the general term formula from this recursive formula is difficult. Therefore, we hope to use some inequalities to simplify this recursive relationship and thus bound $\alpha^R_{\{\gamma_i\gamma_j\},2t+1}$ by $\alpha^L_{\{\gamma_i\gamma_j\},2t+1}$.

We will first define some auxiliary variables,

$$\zeta_k(t) := \frac{1}{2}\sum_{\mu=1}^{N-k}\left(\mathcal{L}_i(\mu,t)\mathcal{L}_j(\mu+k,t) + \mathcal{L}_i(\mu+k,t)\mathcal{L}_j(\mu,t)\right)$$

$$\beta_k(t) := \frac{1}{2}\sum_{\mu=1}^{N-k}\left(\mathscr{R}_{i,j}(\mu,\mu+k,t) + \mathscr{R}_{i,j}(\mu+k,\mu,t)\right)$$

$$a(t) := \begin{pmatrix}\zeta_0(t)\\ \zeta_1(t)\end{pmatrix}, \quad b(t) := \begin{pmatrix}\beta_0(t)\\ \beta_1(t)\end{pmatrix}.$$

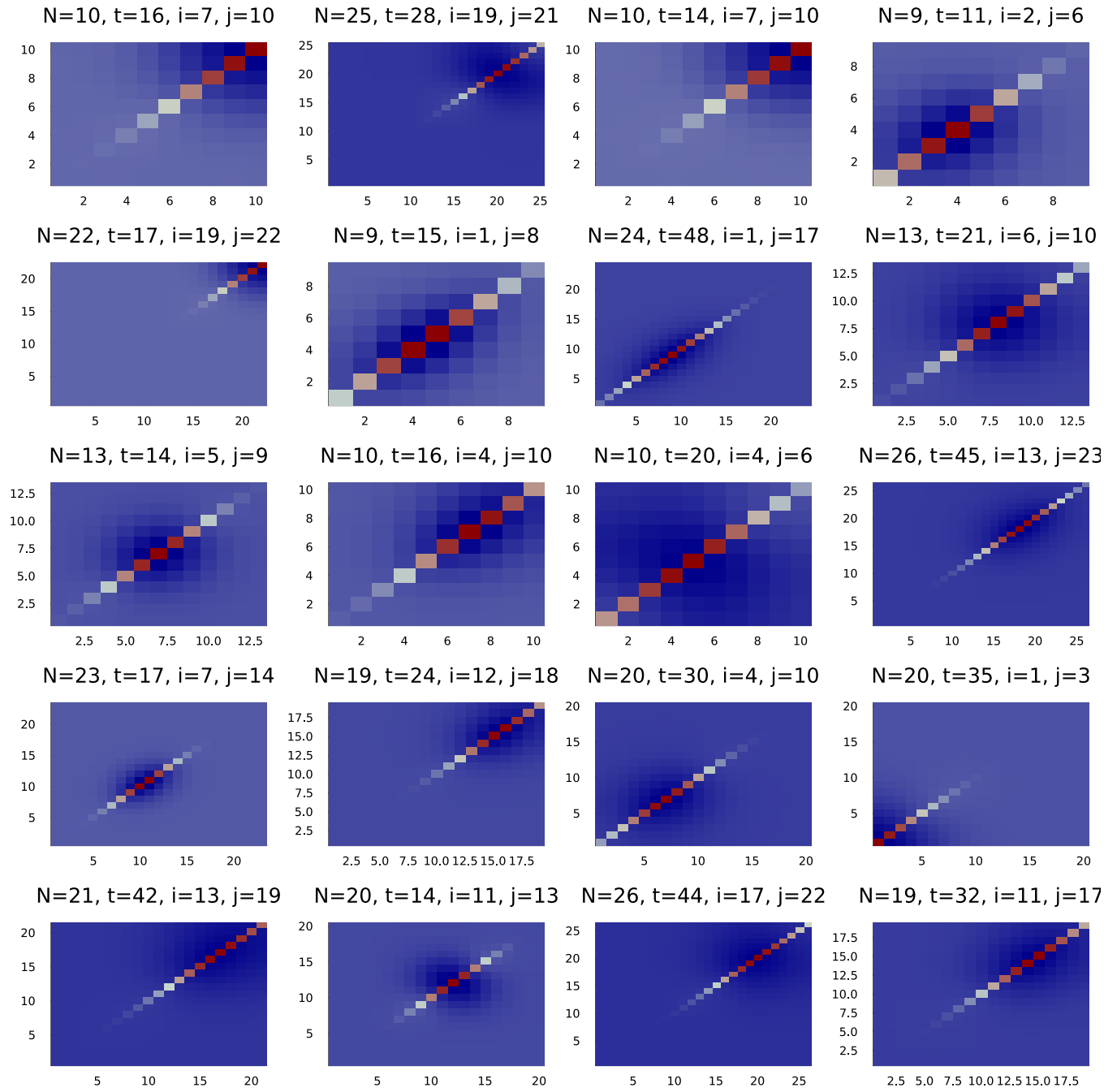

FIG. 8: Numerical evaluation of $\mathscr{R}_{i,j}(\mu,\nu,t)$ by randomly choosing N,t,i,j. The pixel is colored red if $\mathscr{R}_{i,j}(\mu,\nu,t)$ is smaller than 0 and blue otherwise. The x-axis represents the value of μ, and the y-axis represents the value of ν. The results indicate that $\mathscr{R}_{i,j}(\mu,\mu,t) < 0$ when $\mu \neq \nu$.

Notice that $3\alpha^L_{\{\gamma_i\gamma_j\},2t+1} = \zeta_0(t)$, $3\alpha^R_{\{\gamma_i\gamma_j\},2t+1} = \beta_0(t)$. Because $\mathscr{L}_{i,j}(\mu,\nu,t) + \mathscr{R}_{i,j}(\mu,\nu,t)$ represents the probability of being in site y_iy_j during a random walk, it satisfies the property that the summation across all sites is 1. Meanwhile, the summation of all $\mathscr{L}_{i,j}(\mu,\nu,t)$ is 1. The two things deduce that

$$\sum_{\mu,\nu} \mathscr{R}_{i,j}(\mu,\nu,t) = 0. \tag{G10}$$

Especially, in numerical simulation, we observe that all $\mathscr{R}_{i,j}(\mu,\nu,t)$ are greater than 0 except for $\mu = \nu$. The numerical results are shown in Fig. 8. Under this assumption, we have the following lemma:

Lemma 7. *Assume that* $\forall \mu \neq \nu$, $\mathscr{R}_{i,j}(\mu,\nu,t) \geq 0$, *and* $\forall \mu \neq \nu$, $\mathscr{R}_{i,j}(\mu,\mu,t) \leq 0$. $-\beta_0(t) \leq \frac{25}{72}\max_{k\geq 0}\{\zeta_0(t-k)\}$.

Lemma 7 establishes the mathematical relationship between the two components $\alpha^L_{\{\gamma_i\gamma_j\},2t+1}$ and $\alpha^R_{\{\gamma_i\gamma_j\},2t+1}$. By combining this theoretical relationship with the equality described in Eq. (E31), we can deduce the order of magnitude of the $\alpha_{\{\gamma_i\gamma_j\},2t+1}$. Combining these pieces allows us to systematically determine the scale or size of $\alpha_{\{\gamma_i\gamma_j\},2t+1}$ based on the other defined quantities.

proof of Lemma 7. From the recursive relationship in Eq. (G9) and Table II, we can write down the recursive relationship of β_k

$$\begin{aligned}
\beta_0(t+1) \geq\ & \frac{6}{16}\beta_0(t) + \frac{8}{16}\beta_1(t) + \frac{2}{16}\beta_2(t) - \frac{14}{144}\left(\beta_0(t)+\zeta_0(t)\right) - \frac{1}{24}\left(\beta_1(t)+\zeta_1(t)\right) \\
& + \frac{4}{16}(\mathscr{R}_{ij}(0,0,t-1)+\mathscr{R}_{ij}(N,N,t-1)) - \frac{1}{16}(\mathscr{R}_{ij}(0,1,t-1)+\mathscr{R}_{ij}(1,0,t-1)) \\
& - \frac{1}{16}(\mathscr{R}_{ij}(N-1,N,t-1)+\mathscr{R}_{ij}(N,N-1,t-1)) \\
\geq\ & \frac{5}{18}\beta_0(t) + \frac{11}{24}\beta_1(t) - \frac{7}{72}\zeta_0(t) - \frac{1}{12}\zeta_1(t) \qquad \text{(G11)} \\
\geq\ & \frac{5}{18}\beta_0(t) + \frac{5}{24}\beta_1(t) - \frac{7}{72}\zeta_0(t) - \frac{1}{12}\zeta_1(t) \qquad \text{(G12)}
\end{aligned}$$

Here, we use the property that $\beta_0(t)+\zeta_0(t)$ is the summation of properties so that it is greater than 0 to inequality deflate the terms at the edges, like y_0y_0 or y_0y_1. Recall that we hold the assumption that $\mathscr{R}_{i,j}(\mu,\mu,t) < 0$, and $\forall \mu \neq \nu$, $\mathscr{R}_{i,j}(\mu,\mu,t) > 0$, so the edges terms of $\mathscr{R}_{ij}$ can be deflated out as well. Similarly, we have

$$\beta_1(t+1) \geq \frac{5}{9}\beta_0(t)+\frac{5}{12}\beta_1(t)+\frac{1}{18}\zeta_0(t)+\frac{1}{24}\zeta_1(t). \quad \text{(G13)}$$

Let β'_0 and β'_1 obtains the above recursive relation

$$\begin{cases} \beta'_0(t+1) = & \frac{5}{18}\beta_0(t) + \frac{5}{24}\beta_1(t) - \frac{7}{72}\zeta_0(t) - \frac{1}{12}\zeta_1(t) \\ \beta'_1(t+1) = & \frac{5}{9}\beta_0(t) + \frac{5}{12}\beta_1(t) + \frac{1}{18}\zeta_0(t) + \frac{1}{24}\zeta_1(t) \end{cases} \quad \text{(G14)}$$

with the same first term $\beta'_0(0) = \beta_0(0)$ and $\beta'_1(0) = \beta_1(0)$. The β and β' satisfy the relationship

$$\beta'_0(t) \geq \beta_0(t), \quad \beta'_1(t) \geq \beta_1(t). \quad \text{(G15)}$$

Similarly, we denote b' as $b'(t) := \binom{\beta'_0(t)}{\beta'_1(t)}$,

We rewrite the inequality groups (G14) to the matrix form

$$b'(t+1) = C_b b'(t) + C_a a(t), \quad \text{where} \quad \text{(G16)}$$

$$C_b = \begin{pmatrix} \frac{5}{18} & \frac{5}{24} \\ \frac{5}{9} & \frac{5}{12} \end{pmatrix}, \quad C_a = \begin{pmatrix} -\frac{7}{72} & -\frac{1}{12} \\ \frac{1}{18} & \frac{1}{24} \end{pmatrix}, \quad \text{(G17)}$$

and the matrices C_b and C_a govern these recursive dynamics. To solve this recursion explicitly, we diagonalize the C_b matrix. The term C_b^t can be calculated by eigenvalue decomposition $C_b = Q\Lambda Q^{-1}$, where $\Lambda = \mathrm{diag}(\frac{25}{36}, 0)$. The eigenvector corresponding to $\frac{25}{36}$ is $(2, \frac{3}{2})^T$, where T denotes the transpose of vector. This allows us to express C_b^k and $C_b^k C_a$ in terms of eigenvalues and eigenvectors

$$C_b^k = \left(\frac{5}{6}\right)^{2k}\begin{pmatrix} 2 & \frac{3}{2} \\ 0 & 0 \end{pmatrix} \quad \text{(G18)}$$

$$C_b^k C_a = \frac{1}{5}\left(\frac{5}{6}\right)^{2k}\begin{pmatrix} -\frac{1}{9} & -\frac{5}{48} \\ 0 & 0 \end{pmatrix} \quad \text{(G19)}$$

for any $k > 0$.

The variables we care about are ζ_0 and β_0 because they are directly related to the $\alpha^L_{\{\gamma_i\gamma_j\},2t+1}$ and $\alpha^R_{\{\gamma_i\gamma_j\},2t+1}$. Thus, we mainly consider the first item of $C_b^t b'(0)$ and $C_b^k C_a a(t-k-1)$, which can be expressed in the following form

$$C_b^k C_a a(t-k-1) = \lambda_k\zeta_0(t-k-1)+\eta_k\zeta_1(t-k-1). \quad \text{(G20)}$$

The λ_k and the η_k are coefficients

$$\begin{aligned} &\lambda_k = -\tfrac{1}{45}\left(\tfrac{5}{6}\right)^{2k}, \quad \eta_k = -\tfrac{1}{48}\left(\tfrac{5}{6}\right)^{2k}, \quad \forall k > 0, \\ &\lambda_0 = -\tfrac{1}{72}, \qquad\qquad \eta_0 = -\tfrac{1}{12}. \end{aligned} \quad \text{(G21)}$$

Building on the previous relationships, we can now derive an explicit formula for $\beta'_0(t)$. From the expression for the first element of $C_b^k C_a a(t-k-1)$, we obtain

$$\beta'_0(t) = \sum_{k=0}^{t}\left(\lambda_k\zeta_0(t-k-1)+\eta_k\zeta_1(t-k-1)\right) \quad \text{(G22)}$$

We also know from the recursive relation of $\mathcal{L}_i$ that the state variables satisfy

$$\zeta_0(t+1) \geq \frac{3}{8}\zeta_0(t) + \frac{1}{2}\zeta_1(t). \quad \text{(G23)}$$

Leveraging this inequality into Eq. G22 allows us to place an upper bound on $\beta'_0(t)$

$$-\beta_0'(t) \leq -\sum_{k=1}^{t}\left(\lambda_k - \frac{3}{4}\eta_k + 2\eta_{k+1}\right)\zeta_0(t-k-1) + \frac{19}{72}\zeta_0(t) - \frac{1}{16}\zeta_0(t-1) \tag{G24}$$

$$\leq \sum_{k=1}^{t}\left(\frac{5}{6}\right)^{2k}\frac{307}{8640}\zeta_0(t-k-1) + \frac{19}{72}\zeta_0(t) - \frac{1}{16}\zeta_0(t-1) \tag{G25}$$

$$\leq \frac{25}{72}\max_{k\geq 0}\{\zeta_0(t-k)\}\,. \tag{G26}$$

□

Combine Lemma 4 and Lemma 7, we conclude the following theorem:

Theorem 1. *The sample complexity scales $\mathcal{O}(\frac{n}{\epsilon^2})$ up to a log factor for 2-local Majorana strings in the average of ρ when the depth satisfies*

$$d^* = \Theta\left(\max\left\{\frac{d_{int}(S)^2}{\log(n)}, d_{int}(S)\right\}\right) \tag{G27}$$

under the following assumption: Compared to the SLRW, the true random walk in polynomial space $\mathcal{P}_N$ (The random walk of $\varphi'\circ\phi(\gamma_S)$ under transition $\mathcal{B}$) has less probability to walks on the diagonal sites y_iy_j but has larger probability to walks on the off-diagonal sites at step t.

Proof. As we have discussed, the sample complexity is decided by $\alpha_{S,d}$, which can be expanded by

$$\alpha_{S,d} = \alpha^L_{S,d} + \alpha^R_{S,d}. \tag{G28}$$

The assumption about the random walk means

$$\begin{cases}\mathscr{R}_{i,j}(\mu,\mu,t) \leq 0,\\ \mathscr{R}_{i,j}(\mu,\nu,t) \geq 0, \forall \mu \neq \nu.\end{cases} \tag{G29}$$

Following Lemma 7, we have

$$\alpha_{S,d} = \alpha^L_{S,d} + \alpha^R_{S,d} \tag{G30}$$

$$\geq \alpha^L_{S,d} - \frac{25}{72}\max_{d'<d}\{\alpha^L_{S,d'}\} \tag{G31}$$

$$\geq \frac{47}{72}\max_{d'\leq d}\{\alpha^L_{S,d'}\}. \tag{G32}$$

If $a = \mathcal{O}(\log n)$, the proof is complete by Lemma 8 with depth $d^* = \Theta(|i-j|)$. For $a = \omega(\log n)$, we have $\mathcal{O}(e^{-\pi^2 d}) = \mathcal{O}(n^{-\pi^2})$, and $\frac{1}{\sqrt{2\pi t}}e^{-\frac{(i-j)^2}{2t}} = \Omega(n)$ up to a log factor. In this case, we show that $\alpha^L_{S,d} = \Omega(n)$ with a similar method used in Lemma 5. Combine Chebyshev inequality and inequality (13), and we conclude that the sample complexity is $\mathcal{O}(\frac{n}{\epsilon^2})$. □

Appendix H: Efficiency when the distance of set is short

Lemma 8. *The expectation value of $\mathrm{tr}(\rho\gamma_S)$ can be obtained by using $\mathcal{O}(\log(n))$-depth matchgate circuit within the Fermionic classical shadows protocol when the distance of S is $\mathcal{O}(\log n)$ and the cardinal number $|S| = 2k$ is a constant.*

Proof. Let the initial tensor be P_S, and apply $\mathcal{C}$ to the tensor P_S. Each $\mathcal{B}$ in $\mathcal{C}$ will transform the P_S to the superposition of a series of Pauli tensors

$$\mathcal{B}|P_S, P_S\rangle\rangle = \sum_{|S'|=|S|}\xi_{S'}|P_{S'}, P_{S'}\rangle\rangle, \tag{H1}$$

where $\xi_{S'}$ are real coefficients that satisfy $\sum\xi_{S'} = 1$, and the concrete number of $\xi_{S'}$ are shown in Table I. The tensor network contraction of $\alpha_{S,d}$ contracts out the outputs supervectors $|\mathcal{Z}\rangle\rangle$. The supervectors $|P_{S'}, P_{S'}\rangle\rangle$ in the output state $\mathcal{C}|P_S, P_S\rangle\rangle = \sum_{|S'|=|S|}\xi^C_{S'}|P_{S'}, P_{S'}\rangle\rangle$ make non-zero contribution to the $\alpha_{S,d}$ only if it just contains Pauli $\mathbb{1}$ or I operators. Thus, at each step, we only preserve the branches S' which has the trend to arrive $|P_{S'}, P_{S'}\rangle\rangle$ with $\mathbb{1}$ or I. Formally, for each transition $\mathcal{B}$, we follows:

1. preserves $|P_{S'}, P_{S'}\rangle\rangle$ if $d_{\mathrm{near}}(S') \leq d_{\mathrm{near}}(S)$
2. discards $|P_{S'}, P_{S'}\rangle\rangle$ (let $\xi_{S'} = 0$) if $d_{\mathrm{near}}(S') > d_{\mathrm{near}}(S)$

where $d_{\mathrm{near}}(S) := \max\{i_{2j} - i_{2j-1} \mid j \in [n]\}$.

Table I tells us two facts:

1. There exist a S' such that $d_{\mathrm{near}}(S') = d_{\mathrm{near}}(S) - m$ for S with $d_{\mathrm{near}}(S) \geq m$, $m \leq 2$.
2. the summation of $\xi_{S'}$ for remaining branches is greater than $\frac{1}{36^k}$.

Thus, with $d_{\mathrm{near}}(S)/2$ steps, there exists a S' such that the $\xi_{S'}$ is non-zero. Since $d_{\mathrm{int}}(S) \geq d_{\mathrm{near}}(S)$, the summation of coefficients of the remaining branches is greater than $\frac{1}{36^{k d_{\mathrm{int}}(S)/2}}$ after $d_{\mathrm{int}}(S)/2$ steps transition. Notice that $|S| = k$ is a constant number and $d_{\mathrm{int}}(S) = \mathcal{O}(\log(n))$, the summation number is

$$\sum_{S''}\xi_{S''} \geq \frac{1}{36^{k d_{\mathrm{int}}(S)/2}} = \frac{1}{\mathcal{O}(n^{k/2}\mathrm{polylog}(n))} \tag{H2}$$

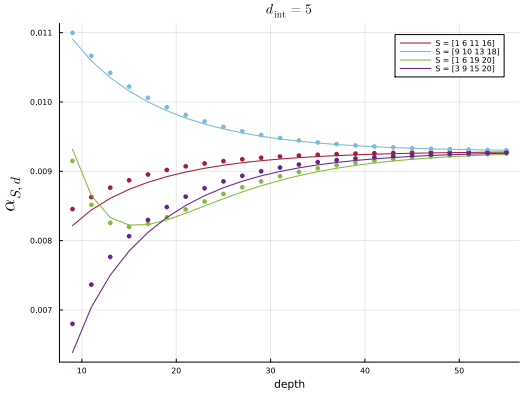

FIG. 9: Values of $\alpha_{S,d}$ and $\alpha'_{S,d}$ with the same d_{int} and different S.

where S'' are the remaining branches. □

Appendix I: More data for numerical simulation

Fig. 9 shows the values of $\alpha_{S,d}$ and $\alpha'_{S,d}$ with the same d_{int} and different S. The optimal depth d^* depends on the d_{int}, which means the four different curves share the same optimal depth order. Although the values $\alpha'_{S,d}$ are different for different S, depth d^* promises that for all sets S with the same d_{int} scales polynomially small.

[1] Elliott Lieb, Theodore Schultz, and Daniel Mattis. Two soluble models of an antiferromagnetic chain. *Annals of Physics*, 16(3):407–466, 1961.

[2] Qimiao Si and J Lleweilun Smith. Kosterlitz-thouless transition and short range spatial correlations in an extended hubbard model. *Physical review letters*, 77(16):3391, 1996.

[3] Alán Aspuru-Guzik, Anthony D Dutoi, Peter J Love, and Martin Head-Gordon. Simulated quantum computation of molecular energies. *Science*, 309(5741):1704–1707, 2005.

[4] James D Whitfield, Jacob Biamonte, and Alán Aspuru-Guzik. Simulation of electronic structure hamiltonians using quantum computers. *Molecular Physics*, 109(5):735–750, 2011.

[5] Assa Auerbach. *Interacting electrons and quantum magnetism*. Springer Science & Business Media, 2012.

[6] Yudong Cao, Jonathan Romero, Jonathan P Olson, Matthias Degroote, Peter D Johnson, Mária Kieferová, Ian D Kivlichan, Tim Menke, Borja Peropadre, Nicolas PD Sawaya, et al. Quantum chemistry in the age of quantum computing. *Chemical reviews*, 119(19):10856–10915, 2019.

[7] Jules Tilly, Hongxiang Chen, Shuxiang Cao, Dario Picozzi, Kanav Setia, Ying Li, Edward Grant, Leonard Wossnig, Ivan Rungger, George H Booth, et al. The variational quantum eigensolver: a review of methods and best practices. *Physics Reports*, 986:1–128, 2022.

[8] Marco Cerezo, Andrew Arrasmith, Ryan Babbush, Simon C Benjamin, Suguru Endo, Keisuke Fujii, Jarrod R McClean, Kosuke Mitarai, Xiao Yuan, Lukasz Cincio, et al. Variational quantum algorithms. *Nature Reviews Physics*, 3(9):625–644, 2021.

[9] William MC Foulkes, Lubos Mitas, RJ Needs, and Guna Rajagopal. Quantum monte carlo simulations of solids. *Reviews of Modern Physics*, 73(1):33, 2001.

[10] Joseph Carlson, Stefano Gandolfi, Francesco Pederiva, Steven C Pieper, Rocco Schiavilla, Kevin E Schmidt, and Robert B Wiringa. Quantum monte carlo methods for nuclear physics. *Reviews of modern physics*, 87(3):1067–1118, 2015.

[11] Hsin-Yuan Huang, Richard Kueng, and John Preskill. Predicting many properties of a quantum system from very few measurements. *Nature Physics*, 16(10):1050–1057, 2020.

[12] Xavier Bonet-Monroig, Ryan Babbush, and Thomas E O'Brien. Nearly optimal measurement scheduling for partial tomography of quantum states. *Physical Review X*, 10(3):031064, 2020.

[13] Andrew Zhao, Nicholas C. Rubin, and Akimasa Miyake. Fermionic partial tomography via classical shadows. *Physical review letters*, 127:110504, Sep 2021.

[14] Guang Hao Low. Classical shadows of fermions with particle number symmetry. *arXiv preprint arXiv:2208.08964*, 2022.

[15] Kianna Wan, William J. Huggins, Joonho Lee, and Ryan Babbush. Matchgate shadows for fermionic quantum simulation, 2022.

[16] Andrew Zhao and Akimasa Miyake. Group-theoretic error mitigation enabled by classical shadows and symmetries. *npj Quantum Information*, 10(1):57, 2024.

[17] Valentin Heyraud, Héloise Chomet, and Jules Tilly. Unified framework for matchgate classical shadows. *arXiv preprint arXiv:2409.03836*, 2024.

[18] Ketan N Patel, Igor L Markov, and John P Hayes. Optimal synthesis of linear reversible circuits. *Quantum Information & Computation*, 8(3):282–294, 2008.

[19] Jiaqing Jiang, Xiaoming Sun, Shang-Hua Teng, Bujiao Wu, Kewen Wu, and Jialin Zhang. Optimal space-depth trade-off of cnot circuits in quantum logic synthesis. In *Proceedings of the Fourteenth Annual ACM-SIAM Symposium on Discrete Algorithms*, pages 213–229. SIAM, 2020.

[20] Zhang Jiang, Kevin J Sung, Kostyantyn Kechedzhi, Vadim N Smelyanskiy, and Sergio Boixo. Quantum algorithms to simulate many-body physics of correlated fermions. *Physical Review Applied*, 9(4):044036, 2018.

[21] Frank Arute, Kunal Arya, Ryan Babbush, Dave Bacon, Joseph C Bardin, Rami Barends, Rupak Biswas, Sergio Boixo, Fernando GSL Brandao, David A Buell, et al. Quantum supremacy using a programmable superconducting processor. *Nature*, 574(7779):505–510, 2019.

[22] Yulin Wu, Wan-Su Bao, Sirui Cao, Fusheng Chen, Ming-Cheng Chen, Xiawei Chen, Tung-Hsun Chung, Hui Deng, Yajie Du, Daojin Fan, Ming Gong, Cheng Guo, Chu Guo, Shaojun Guo, Lianchen Han, Linyin Hong, He-Liang Huang, Yong-Heng Huo, Liping Li, Na Li, Shaowei Li, Yuan Li, Futian Liang, Chun Lin, Jin Lin, Haoran Qian, Dan Qiao, Hao Rong, Hong Su, Lihua Sun, Liangyuan Wang, Shiyu Wang, Dachao Wu, Yu Xu, Kai Yan, Weifeng Yang, Yang Yang, Yangsen Ye, Jianghan Yin, Chong Ying, Jiale Yu, Chen Zha, Cha Zhang, Haibin Zhang, Kaili Zhang, Yiming Zhang, Han Zhao, Youwei Zhao, Liang Zhou, Qingling Zhu, Chao-Yang Lu, Cheng-Zhi Peng, Xiaobo Zhu, and Jian-Wei Pan. Strong quantum computational advantage using a superconducting quantum processor. *Physical review letters*, 127:180501, Oct 2021.

[23] Sirui Cao, Bujiao Wu, Fusheng Chen, Ming Gong, Yulin Wu, Yangsen Ye, Chen Zha, Haoran Qian, Chong Ying, Shaojun Guo, et al. Generation of genuine entanglement up to 51 superconducting qubits. *Nature*, 619(7971):738–742, 2023.

[24] Christian Bertoni, Jonas Haferkamp, Marcel Hinsche, Marios Ioannou, Jens Eisert, and Hakop Pashayan. Shallow shadows: Expectation estimation using low-depth random clifford circuits. *Physical Review Letters*, 133(2):020602, 2024.

[25] Thomas Schuster, Jonas Haferkamp, and Hsin-Yuan Huang. Random unitaries in extremely low depth. *arXiv preprint arXiv:2407.07754*, 2024.

[26] Pierre-Gabriel Rozon, Ning Bao, and Kartiek Agarwal. Optimal twirling depth for classical shadows in the presence of noise. *Physical review letters*, 133:130803, Sep 2024.

[27] Fermi Ma and Hsin-Yuan Huang. How to construct random unitaries. *arXiv preprint arXiv:2410.10116*, 2024.

[28] Robbie King, David Gosset, Robin Kothari, and Ryan Babbush. Triply efficient shadow tomography. *arXiv preprint arXiv:2404.19211*, 2024.

[29] Zhang Jiang, Kevin J. Sung, Kostyantyn Kechedzhi, Vadim N. Smelyanskiy, and Sergio Boixo. Quantum algorithms to simulate many-body physics of correlated fermions. *Physical review applied*, 9:044036, Apr 2018.

[30] Martin Greiter, Vera Schnells, and Ronny Thomale. The 1d ising model and the topological phase of the kitaev chain. *Annals of Physics*, 351:1026–1033, 2014.

[31] Umberto Borla, Ruben Verresen, Jeet Shah, and Sergej Moroz. Gauging the kitaev chain. *SciPost Physics*, 10(6):148, 2021.

[32] Annette M Marsolais. The equivalence between the kitaev, the transverse quantum ising model and the classical ising model. Master's thesis, The University of Akron, 2021.

[33] Lucas Hackl and Eugenio Bianchi. Bosonic and fermionic gaussian states from kähler structures. *SciPost Physics Core*, 4(3):025, 2021.

[34] Leslie G. Valiant. Quantum circuits that can be simulated classically in polynomial time. *SIAM Journal on Computing*, 31(4):1229–1254, 2002.

[35] Senrui Chen, Wenjun Yu, Pei Zeng, and Steven T. Flammia. Robust shadow estimation. *PRX Quantum*, 2:030348, Sep 2021.

[36] Ari M. Turner, Frank Pollmann, and Erez Berg. Topological phases of one-dimensional fermions: An entanglement point of view. *Physical review B*, 83:075102, Feb 2011.

[37] Luca Giuggioli. Exact spatiotemporal dynamics of confined lattice random walks in arbitrary dimensions: a century after smoluchowski and pólya. *Physical Review X*, 10(2):021045, 2020.

[38] Gregory F Lawler and Vlada Limic. *Random walk: a modern introduction*, volume 123. Cambridge University Press, 2010.

[39] A Yu Kitaev. Unpaired majorana fermions in quantum wires. *Physics-uspekhi*, 44(10S):131, 2001.

[40] Jonas Haferkamp, Philippe Faist, Naga BT Kothakonda, Jens Eisert, and Nicole Yunger Halpern. Linear growth of quantum circuit complexity. *Nature Physics*, 18(5):528–532, 2022.